

AD A098944

82

LEVEL 4

12

RADC-TR-80-360
In-House Report
December 1980



THEORETICAL AND EXPERIMENTAL STUDIES OF HF DUCTED PROPAGATION

Terence J. Elkins
Kurt Toman
Gary S. Sales

APPROVED FOR PUBLIC RELEASE; DISTRIBUTION UNLIMITED

DTIC
ELECTE
MAY 15 1981
S A

DTIC FILE COPY

ROME AIR DEVELOPMENT CENTER
Air Force Systems Command
Griffiss Air Force Base, New York 13441

81 5 15 052

This report has been reviewed by the RADC Public Affairs Office (PA) and is releasable to the National Technical Information Service (NTIS). At NTIS it will be releasable to the general public, including foreign nations.

RADC-TR-80-360 has been reviewed and is approved for publication.

APPROVED:



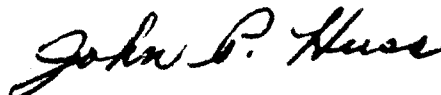
TERENCE J. ELKINS, Acting Chief
Propagation Branch
Electromagnetic Sciences Division

APPROVED:



ALLAN C. SCHELL, Chief
Electromagnetic Sciences Division

FOR THE COMMANDER:



JOHN P. HUSS
Acting Chief, Plans Office

If your address has changed or if you wish to be removed from the RADC mailing list, or if the addressee is no longer employed by your organization, please notify RADC (KEP), Hanscom AFB MA 01731. This will assist us in maintaining a current mailing list.

Do not return this copy. Retain or destroy.

Unclassified

SECURITY CLASSIFICATION OF THIS PAGE (When Data Entered)

| REPORT DOCUMENTATION PAGE | | READ INSTRUCTIONS BEFORE COMPLETING FORM | |
|---|-------------------------------------|--|------|
| 1. REPORT NUMBER RAD-TR-80-360 | 2. GOVT ACCESSION NO. AD-4098944 | 3. RECIPIENT'S CATALOG NUMBER | |
| 4. TITLE (and Subtitle) THEORETICAL AND EXPERIMENTAL STUDIES OF HF DUCTED PROPAGATION | | 5. TYPE OF REPORT & PERIOD COVERED In-house | |
| 7. AUTHOR(s) Terence J. Elkins Kurt/Toman Gary S./Sales | | 6. PERFORMING ORG. REPORT NUMBER | |
| 9. PERFORMING ORGANIZATION NAME AND ADDRESS Deputy for Electronic Technology (RADC/EEP) Hanscom AFB Massachusetts 01731 | | 8. CONTRACT OR GRANT NUMBER 1267 | |
| 11. CONTROLLING OFFICE NAME AND ADDRESS Deputy for Electronic Technology (RADC/EEP) Hanscom AFB Massachusetts 01731 | | 10. PROGRAM ELEMENT, PROJECT, TASK AREA & WORK UNIT NUMBERS 62702F 46001603 | 1716 |
| 14. MONITORING AGENCY NAME & ADDRESS (if different from Controlling Office) | | 12. REPORT DATE December 1980 | |
| | | 13. NUMBER OF PAGES 64 | |
| | | 15. SECURITY CLASS. (of this report) Unclassified | |
| | | 15a. DECLASSIFICATION DOWNGRADING SCHEDULE | |
| 16. DISTRIBUTION STATEMENT (of this Report) Approved for public release; distribution unlimited. | | | |
| 17. DISTRIBUTION STATEMENT (of the abstract entered in Block 20, if different from Report) | | | |
| 18. SUPPLEMENTARY NOTES | | | |
| 19. KEY WORDS (Continue on reverse side if necessary and identify by block number) High frequency Scattering Radio Round the world Ducted propagation Ionosphere | | | |
| 20. ABSTRACT (Continue on reverse side if necessary and identify by block number) Results of an ionospheric radio propagation experiment are discussed which involved high-frequency ionospheric radars located in California, New York, and Australia, with their radiation aimed toward an artificially modified volume of the ionospheric F-region over Platteville, Colorado. Signals originating from these radars were received at field sites in Los Alamos, New Mexico, and Alamosa, Colorado. It has been surmised that signals could arrive at these sites by several types of propagation → next page | | | |

DD FORM 1473 1 JAN 73 EDITION OF 1 NOV 65 IS OBSOLETE

Unclassified

SECURITY CLASSIFICATION OF THIS PAGE (When Data Entered)

309050

JTG

Unclassified

SECURITY CLASSIFICATION OF THIS PAGE (When Data Entered)

20. Abstract (Continued)

cont → mechanisms; for example, conventional multihop propagation along a great-circle path with or without final-hop scattering from the artificial irregularity volume. In another mechanism, likely to be operative for the Australian transmission, the signal at times was expected to be ducted in the F-region of the ionosphere, arrive at the artificial irregularity volume with the propagation vector being nearly horizontal, and be backscattered toward the receiving sites. For comparison, characteristics of round-the-world signals are identified.

→ Considerations of scattering from artificially induced field-aligned ionospheric irregularities are presented. The interpretation of results is facilitated by a numerical study in which raytracing through computationally specified model ionospheres is employed. Ducting predictions are described using the potential field technique. Propagation losses are estimated from raytracing through ionospheric models. The detection of ducted signals by means of an artificially induced scatter volume is shown to be possible.

↑

Unclassified

SECURITY CLASSIFICATION OF THIS PAGE (When Data Entered)

Preface

Many individuals and organizations contributed to the research reported here: Mr. R. Freymann of the Los Alamos Scientific Laboratories provided generous support in making available the Los Alamos receiving site and other logistic support; the Department of Supply of the Australian Government provided the transmissions from Salisbury; Mr. R. Philbrick of Air Force Geophysics Laboratory made available unpublished satellite data providing ionospheric electron density profiles; the Surveillance Division of RADC provided transmissions from the Ava, NY site; SRI International, under contract to RADC, contributed the resources of the Wide Aperture Radar Facility (WARF), scientific personnel and other logistic support; the Institute of Telecommunications Sciences, under contract to RADC reactivated and operated the Platteville heater, participated in the installation and operation of the receiving sites and performed data analysis; The ARCON corporation under contract to RADC, performed most of the computer programming associated with the ionospheric radio propagation simulation. With so many participants, it is impractical to name all of the individuals involved whose efforts contributed to the project. The authors offer their sincere appreciation and thanks to all of these contributors and their organizations without whom, it need hardly be said, these experiments would have been impossible.

| | |
|--------------------|-------------------------------------|
| Accession For | |
| NTIS GRA&I | <input checked="" type="checkbox"/> |
| DTIC TAB | <input type="checkbox"/> |
| Unannounced | <input type="checkbox"/> |
| Justification | |
| By _____ | |
| Distribution/ | |
| Availability Codes | |
| Dist | Avail and/or Special |
| A | |

Contents

| | |
|--|----|
| 1. INTRODUCTION | 9 |
| 2. GENERAL THEORETICAL CONSIDERATIONS | 11 |
| 2.1 Potential Field Analogy | 12 |
| 2.2 Illustration of Potential Field Techniques | 15 |
| 2.3 Coupling to Duct Mode Propagation | 25 |
| 2.4 Raytracing Through Natural Gradients | 26 |
| 2.5 Scattering from Irregularities | 28 |
| 2.6 Propagation Loss Evaluation | 33 |
| 3. GROUND-BASED PROPAGATION EXPERIMENTS | 35 |
| 3.1 Round-the-World (RTW) Propagation | 35 |
| 3.2 Long-range Propagation | 43 |
| 4. ANALYSIS and INTERPRETATION | 59 |
| 5. CONCLUSION | 60 |
| REFERENCES | 63 |

Illustrations

| | |
|---|----|
| 1. Schematic Display of Chordal and Ducted Mode | 10 |
| 2. Schematic Display of Potential Function for Two-Layer Ionosphere | 13 |

Illustrations

| | |
|--|----|
| 3. Mid-latitude Electron Density Height Profile Averaged from Direct Ion Probe Measurements on Board the Satellite S3-1 | 14 |
| 4. Potential Functions for the Ionosphere of Figure 3 That Display the Changes with Operating Frequency | 15 |
| 5. Computed Time Variation of the Maximum and Minimum of the F-region Critical Frequencies (f_oF_2) Along a Particular Propagation Path for Medium and High Sunspot Number | 16 |
| 6. Computed Electron Density Height Contours Along a Particular Propagation Path | 17 |
| 7. Computed Contours of F-region Critical Frequencies (f_oF_2) Spanned by Distance and Time (UT) for a Particular Propagation Path (SSN = 150) | 18 |
| 8. Computed Contours of F-region Critical Frequencies (f_oF_2) Spanned by Distance and Time (UT) for a Particular Propagation Path (SSN = 50) | 19 |
| 9. Model Plasma Frequency for Three-Layer Ionosphere Varying with Height Above and Range Along a Particular Propagation Path | 20 |
| 10. Isometric Display of Potential Function for Ionosphere of Figure 9 Using Operating Frequency of 20 MHz | 21 |
| 11. Isometric Display of Potential Function of Ionosphere of Figure 9 Using Operating Frequency of 22 MHz | 22 |
| 12. Isometric Display of Potential Function for Ionosphere of Figure 9 Using Operating Frequency of 24 MHz | 23 |
| 13. Curves of the Smallest Negative Values of the Potential Function, for E- and F-region at 16, 18, 20 MHz Along the Propagation Path | 24 |
| 14. Plots of the Adiabatic Invariant for E, EF and F Mode Varying Along the Propagation Path | 25 |
| 15. Progression of Solar Terminator Toward Transmitter | 26 |
| 16. Sequence of Three-Dimensional Numerical Raytracings Through Model Ionosphere at Four Local Times for a Fixed Transmitter | 27 |
| 17. Scattering Geometry for Reradiation of Incident Electromagnetic Waves by Elongated Irregularities | 30 |
| 18. Normalized Reradiated Power as a Function of Scatter Angle for Ranges of Transverse Irregularity Dimension l and Anisotropy η ($\lambda = 10$ m) | 31 |
| 19. Normalized Reradiated Power as a Function of Scatter Angle for Ranges of Transverse Irregularity Dimension l and Anisotropy η ($\lambda = 20$ m) | 31 |
| 20. Computed Wavelength Dependence of Aspect Sensitivity Near Orthogonality ($\theta \rightarrow 0$) | 32 |
| 21. Sample Illustration of Propagation Loss, Computed for Different Transmitter Heights, Over a 10,000 km Propagation Path | 34 |
| 22. Round-the-world Echo of FM/CW Signal Radiated Northward from Ava, NY and Received at Verona, NY About 137.5 msec later | 36 |

Illustrations

| | |
|---|----|
| 23. Observed Maximum and Minimum Frequencies in Megahertz of Round-the-world Echoes and Their Group Delays in Milliseconds | 37 |
| 24. Round-the-world Echo of FM/CW Signal Radiated Eastward from Ava, NY and Received at Los Alamos, New Mexico | 38 |
| 25. Round-the-world Echo of FM/CW Signal Radiated Westward from Ava, NY and Received at Los Alamos, New Mexico | 39 |
| 26. Sep 18, 1978 Ava - Los Alamos. Observed Maximum and Minimum Frequencies in Megahertz of Round-the-world Echoes and Their Group Delays in Milliseconds | 40 |
| 27. Sep 19, 1978 Ava - Los Alamos, Lost Hills - Los Alamos. Observed Maximum and Minimum Frequencies in Megahertz of Round-the-world Echoes and Their Group Delays in Milliseconds | 40 |
| 28. Sep 20, 1978 Ava - Los Alamos. Observed Maximum and Minimum Frequencies in Megahertz of Round-the-world Echoes and Their Group Delays in Milliseconds | 41 |
| 29. Sep 22, 1978 Ava - Los Alamos. Observed Maximum and Minimum Frequencies in Megahertz of Round-the-world Echoes and Their Group Delays in Milliseconds | 41 |
| 30. June 5, 1979 Ava - Los Alamos. Observed Maximum and Minimum Frequencies in Megahertz of Round-the-world Echoes and Their Group Delays in Milliseconds | 42 |
| 31. Preferred Times of Occurrence of Round-the-world Echoes Between Ava, New York and Los Alamos, New Mexico from 18 to 22 Sep 1978 | 42 |
| 32. Layout for High-Frequency Propagation Experiment Utilizing the Ionospheric Heater | 44 |
| 33. Loci of Scattering Cones, Including Refraction, Intersecting the Surface of the Earth | 46 |
| 34. The Azimuthal Configuration Over Platteville, Colorado, Pertaining to the Scattering Loci, the Magnetic Meridian and the Direction Toward Adelaide, Australia | 47 |
| 35. Loci of Scattering Cones with Refraction for $f = 18$ MHz and Two Azimuths Illustrating the Location of the Loci North and South of Los Alamos | 48 |
| 36. Effect of Elevation Angle of Ray Arriving at Irregularity Height with Elevation Angle of $+5^{\circ}$ (from above) and -5° (from below) With Respect to the Horizontal | 49 |
| 37. Wide Aperture Research Facility (WARF) Backscatter Sounding (Shows Direct Scatter from the Heated Volume above Platteville and the Effects of Azimuthal Scanning on the Delay Spread) | 52 |

Illustrations

| | |
|--|----|
| 38. Nighttime Ionograms from SRI's Lost Hills Transmitter for 27 April 1979 (Shows Line-of-sight Echo from the Heated Volume above Platteville When the Heater is On (0740 UT) and Off (0735 UT)) | 54 |
| 39. Map of the World Showing the Great-circle-path Defined by Adelaide and Platteville | 55 |
| 40. Oblique Ionograms for the Australia to Los Banos Propagation Path With Platteville Heater Off (Top) and On (Bottom) | 56 |
| 41. Oblique Ionograms for the Australia to Los Alamos Propagation Path with Platteville Heater Off (Top) and On (Bottom) | 58 |
| 42. Ionospheric Contours Characterized by Plasma Frequency in Megahertz, Derived from Ionospheric Model IONCAP for April, 0700 UT for the Path from Salisbury, Australia to Los Alamos, New Mexico | 59 |

Table

| | |
|--|----|
| 1. Participating Transmitting and Receiving Stations | 44 |
|--|----|

Theoretical and Experimental Studies of HF Ducted Propagation

1. INTRODUCTION

The propagation of high frequency (HF) radio energy in so-called "non-classical" modes, that is, in modes other than the conventional earth-ionosphere hops, has recently attracted a great deal of attention. This report deals with two such propagation modes, the chordal and ducted, often grouped together under the generic term "ducting." Figure 1 illustrates the two different modes schematically; note that the chordal mode is a special case of a ducted mode. Numerical calculations and computer propagation simulations are described. New data on the details of the vertical profile of the lower ionosphere are incorporated into some of these calculations. The question of how HF energy can be coupled into elevated ducts from a ground based source is examined in detail. Absorption losses in ducts are estimated using specially adapted raytracing procedures.

A number of different but related experiments are described in which attempts have been made to measure some of the properties of ducted propagation modes. In some of these, natural ionospheric gradients were used to inject energy into ducts, while in others a high power ionospheric heater/modifier was used as a means of mode coupling.

In 1976, the concept emerged in the Propagation Branch of the Electromagnetic Sciences Division to examine the possibility of using low-loss ionospheric

(Received for publication 21 November 1980)

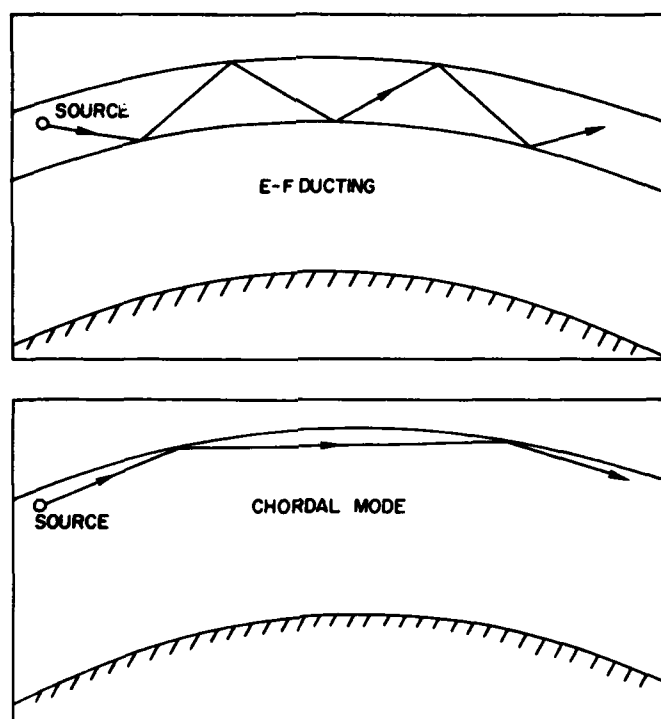


Figure 1. Schematic Display of Chordal and Ducted Mode

ducting channels for propagating electromagnetic signals to large distances. The prediction for the availability of such naturally occurring ducts, based on idealized global ionospheric conditions had already been established.¹ Viewing the ionosphere as a refractive medium, one observes that favorable horizontal ionization gradients are needed for rays to enter an elevated duct from a ground-based source.² In practice, such favorable gradients are available at certain hours of the day depending on location and their estimated local occurrence rate is about 12 percent. Favorable gradients in the general vicinity of a transmitter may lead to the capture of a sufficient portion of the electromagnetic signal in a naturally occurring duct. To receive such a signal on the ground at great distances from the source would require either favorable positive gradients associated with horizontal ionization enhancement in the direction of propagation that

1. Tushentsova, I.A., Fishchuk, D.I., Tzedilina, Ye. Ye. (1975) Investigation of the global properties of ionospheric wave ducts, 2, Geomagn. Aeron. 15(1):62-66.
2. Toman, K., Miller, D.C. (1977) Computational study of long-range high-frequency ionospheric ducting, Radio Science 12(3):467-476.

could bend a ray enough to reach the ground, or ionospheric irregularities that might scatter a substantial portion of the electromagnetic signal to a receiver at the ground.

Prevailing ionospheric ducting channels may not always be accessible to transmissions originating from the ground. Local modification of the ionosphere by radio frequency heating creates, however, ionospheric irregularities that could, by a scattering process, deflect radio energy into an existing, elevated ionospheric duct.³ Conversely, electromagnetic signals already trapped in such a long-range duct could be ejected from the duct toward the ground by natural and artificially induced ionospheric irregularities.

While in certain applications ionospheric modification may eventually be required near both ends of a propagation path, the study described here was conceived to examine the feasibility of successfully using an available radio frequency heater to eject, with artificially created ionospheric irregularities, ducted signals to the ground. For the path from Adelaide, Australia to Los Alamos, advantage was taken of favorable ionospheric gradients near the transmitter site at sunset. Conditions were enhanced by favorable gradients associated with the equatorial anomaly in the F-region ionosphere.

2. GENERAL THEORETICAL CONSIDERATIONS

In order to estimate the characteristics, availability, and behavior of ionospheric ducting channels, several techniques are available, each having its own advantages and limitations. These techniques can be distinguished as 1) Numerical raytracing through model ionospheres considered representative of conditions occurring in nature; 2) μr -diagram obtained for a representative ionospheric profile of a spherically symmetric medium without magnetic field and without collisions; 3) potential field analogy for a representative ionospheric profile of a spherically symmetric medium and its generalization to apply to an inhomogeneous medium. Departures from spherical symmetry generally pose no problems to numerical raytracing but tend to invalidate the use of the potential field approach when inhomogeneities become severe. The μr -diagram remains strictly applicable to a spherically symmetric medium only.

It is believed that the limitation imposed on the validity of raytracing is less stringent than the constraint of the medium's spherical symmetry. Over the short distances within which sudden changes in the refractive index would restrict

3. Gurevich, A.V., Tzedilina, Ye.Ye. (1976) Trapping of radiation in the ionospheric duct during scattering on artificial inhomogeneities, Geomagn. Aeron. 15(6):713-715.

the use of raytracing, specification of the medium is not easily accomplished in practice. When a propagation medium is specified for the purpose of raytracing, care is taken in applying mathematical algorithms and profile specification functions for multiple layers to assure that the refractive index varies slowly in all directions.

2.1 Potential Field Analogy

The propagation of radio waves in ionospheric ducts may be treated in a manner analogous to the trapping of nuclear particles in a potential field well.⁴ Let $U(h) = -\epsilon(h)$ describe the field intensity as a function of altitude, h , where

$$\epsilon(h) = 1 - \frac{\omega_o^2(h)}{\omega^2} + \frac{2h}{R_o}$$

and

ω = wave frequency

ω_o = ionospheric plasma frequency $\sim \sqrt{N_e(h)}$

$N_e(h)$ = vertical profile of electron density

R_o = earth radius

If $\alpha(h)$ is the local elevation angle of the ray direction at height h , then by Snell's law:

$$\epsilon(h) \cos^2 \alpha(h) = \text{constant}$$

For energy trapped in an E-F duct, with reflection at h_1 , then $\alpha(h_1) = 0$, and the maximum value of α in the duct is given by

$$\cos \alpha_{\max} = \left(\frac{\epsilon_{\min}(h)}{\epsilon_{\max}(h)} \right)^{1/2}$$

4. Gurevich, A. V. (1971) Effect of nonlinearity on the generation of circum-terrestrial signals, Geomagn. Aeron. 11(6):810-817.

An adiabatic invariant can be similarly defined, for a frequency f , as

$$I(f) = \frac{r_o}{\cos \alpha_{\max}} \cdot \int_{h_{\min}}^{h_{\max}} [\epsilon(h, f) - \epsilon_{\min}(h, f)]^{1/2} dh$$

The value of the adiabatic invariant is proportional to the energy density in the propagating mode at the frequency in question.

Figure 2 illustrates the form of the function $\epsilon(h)$ for a typical vertical profile, $N_e(h)$. In this example, energy may be trapped in two altitude regions corresponding to two different ranges of the potential function. These two ducting modes are illustrated in Figure 1, in which radio energy is shown respectively trapped between the E and F layers of the ionosphere and propagating via a glancing or chordal mode on the underside of the F-layer.

Figure 3 shows the average ionospheric electron density profile in mid-latitudes as measured by a direct ion probe on board the satellite S3-1. * This profile, as indicated, is typical of the latitude range 45° to 60° at low magnetic activity level ($K_p = 0-2$) and for solar zenith angles ($70^\circ < \chi < 90^\circ$). Note the

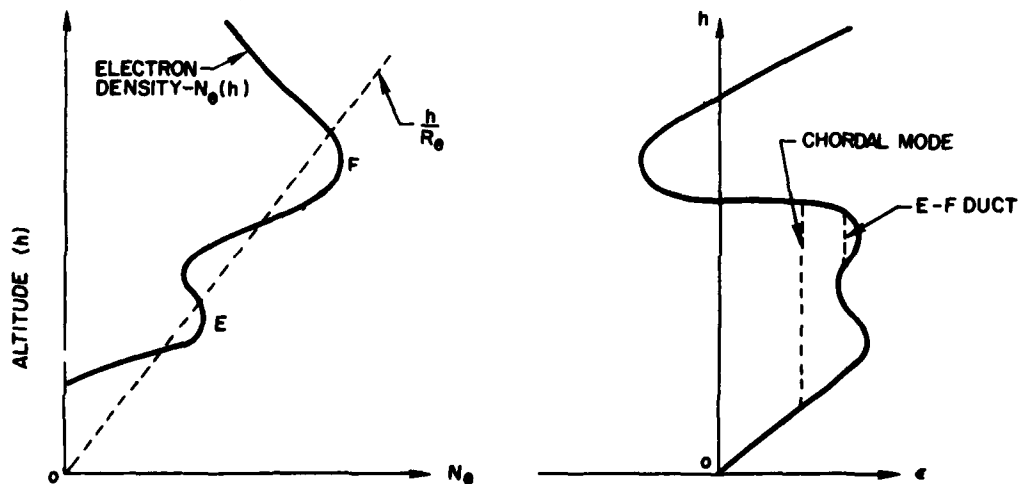


Figure 2. Schematic Display of Potential Function for Two-layer Ionosphere

* R. Philbrick, Private Communication.

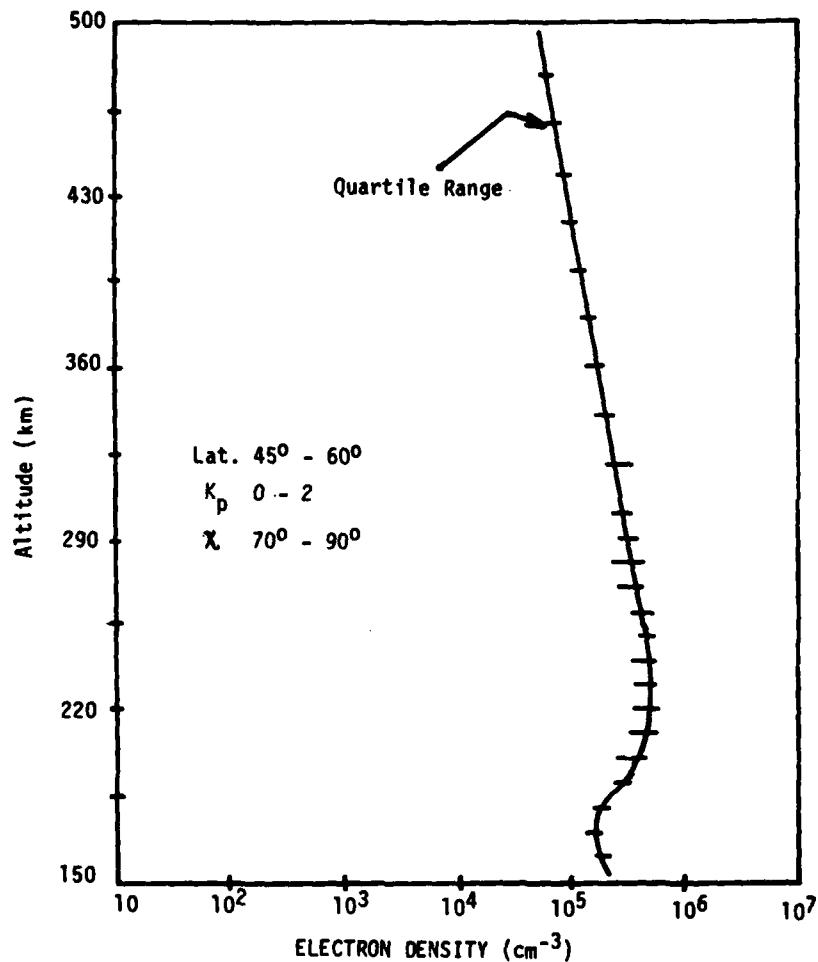


Figure 3. Mid-latitude Electron Density Height Profile Averaged from Direct Ion Probe Measurements on Board the Satellite S3-1

well-defined "valley" at about 180 km, between the E and F regions, which can be expected to support a ducted mode. Figure 4 shows the value of $\epsilon(h)$ plotted as a function of altitude for the profile of Figure 3, for several values of radio frequency between 10 and 30 MHz. The potential well at 170 km altitude can be seen to decrease in intensity, as expected, as the frequency increases.

While the description of radio wave ducting in terms of a potential well is a useful one, there is this limitation: that the potential function depends on one spatial variable only, and thus only a spherically stratified ionosphere can be considered. This simplification excludes the treatment of coupling of energy between a ducted mode and a ground-based transmitter or receiver (in Figure 1,

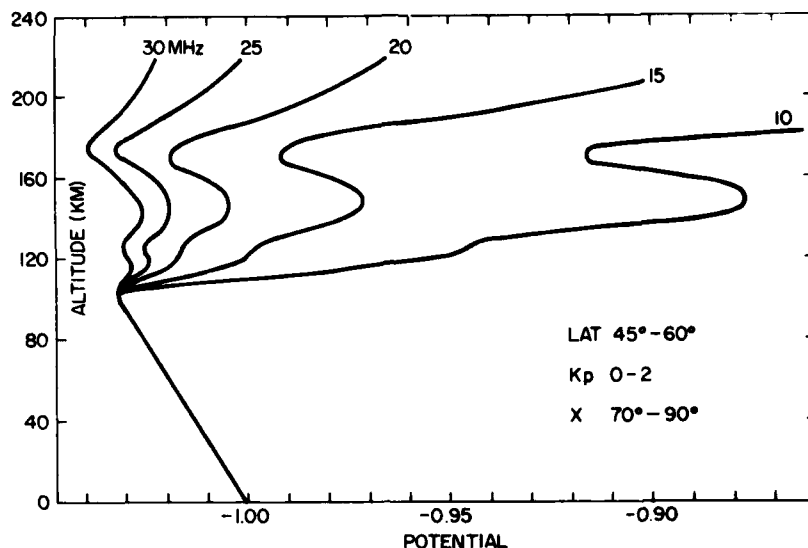


Figure 4. Potential Functions for the Ionosphere of Figure 3 That Display the Changes With Operating Frequency

the source of energy is shown located in the duct). An advantage of the potential well analogy is its simplicity, which permits the convenient estimation, for example, of the global ducting properties of the ionosphere from maps of predicted ionospheric critical frequencies.

2.2 Illustration of Potential Field Techniques

In order to illustrate the value of the potential field technique in estimating the likelihood of ionospheric ducting over large distances, an example is presented here. A transmitter is postulated at a mid-latitude location (28°N ; 183°E) with a beam oriented 45° West of North (azimuth 315°). The ionosphere was modelled along this path using the parameters of the CCIR ionospheric model. Models were constructed for an equinox month (March) at 00, 06, 12, 18 UT for Sunspot Numbers (SSN) of 50 (medium) and 150 (high). Figure 5 shows, for example, the UT dependence of the maximum and minimum critical frequencies (f_oF_2) along the propagation path. Figure 6 shows the variation with range along the direction of propagation of the height profile of plasma density, at UT = 00, SSN = 150. Range is expressed in earth centered degrees ($180^{\circ} \simeq 22,000 \text{ km}$) and plasma density in ($\text{cm}^{-3} \times 10^{-5}$). At UT = 0, the transmitter is close to local noon; sunset occurs at a range of about 70° , and the equatorial anomaly is seen roughly centered at about 130° in the nighttime ionosphere. Figures 7 and 8 show contours of f_oF_2 as functions of range and UT for Sunspot Numbers 150 and

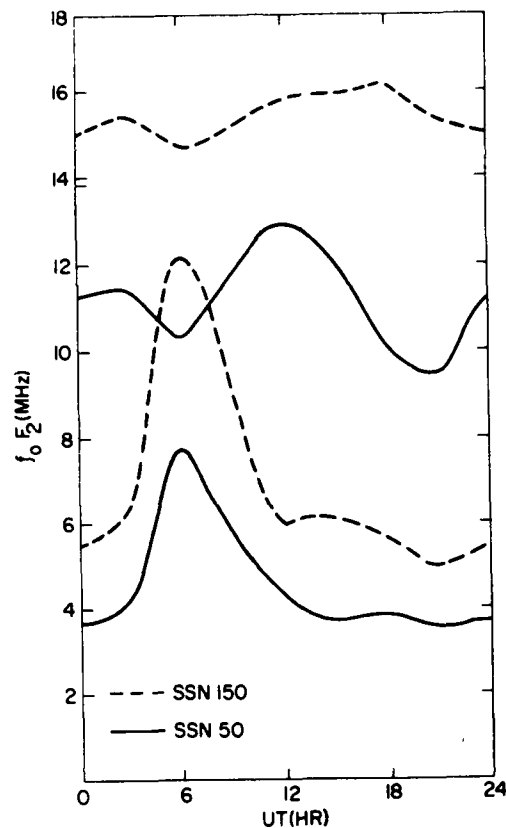


Figure 5. Computed Time Variation of the Maximum and Minimum of the F-region Critical Frequencies ($f_o F_2$) Along a Particular Propagation Path for Medium and High Sunspot Number

50, respectively. Also indicated on these plots are the regions of day and night, the latter shown shaded. The altitude variation of plasma frequency along the direction of propagation is shown in an isometric format in Figure 9 for 00 UT at SSN = 150. The maximum values of the three layers ($f_o E$, $f_o F_1$ and $f_o F_2$) are indicated by heavy solid lines.

The potential function corresponding to Figure 9 is shown in Figures 10, 11, and 12 for frequencies 20, 22, and 24 MHz, respectively. From the transmitter out to a range of 7,200 km, in the daytime ionosphere, classical hop type E and F modes are in evidence as well as E-F ducted energy, depending on the elevation angle and frequency. At night (for ranges greater than 7,200 km) only classical

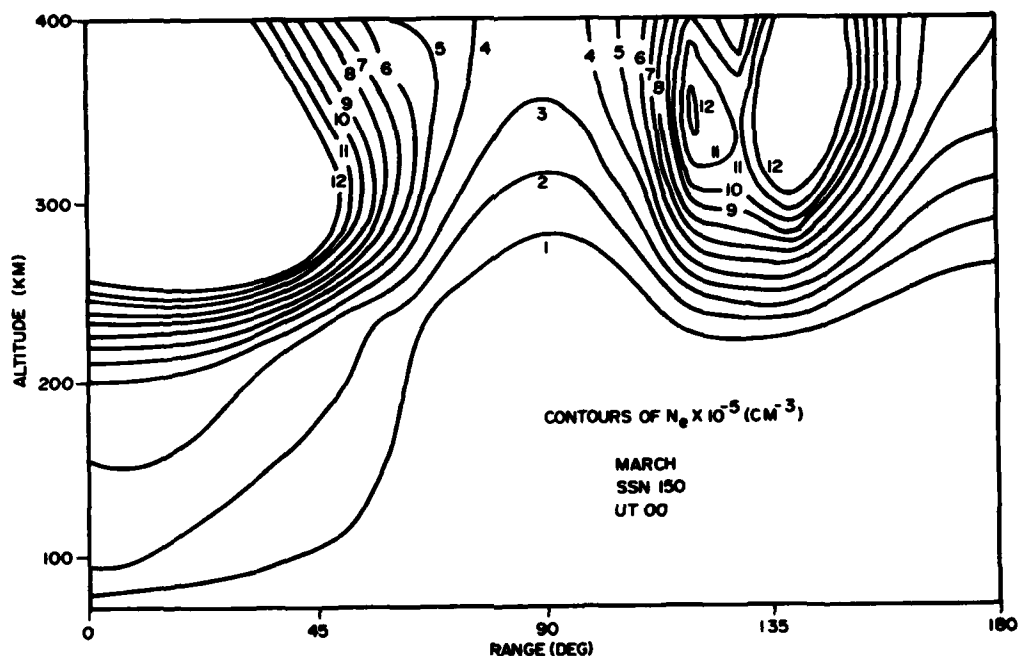


Figure 6. Computed Electron Density Height Contours Along a Particular Propagation Path

F-mode and ducted F (that is, chordal) propagation is possible. In Figure 10, corresponding to a frequency of 20 MHz, the boundaries of the various modes are indicated by heavy solid lines; progressing from the lowest altitudes upwards, these lines indicate (1) lower boundary of chordal E mode, (2) upper boundary of chordal E, or lower boundary of E-F ducted mode, (3) upper boundary of E-F ducting, and (4) upper boundary of chordal F. For example, in Figure 10, an E-F duct exists out to range 7,200 km, while a chordal E mode is possible between 3,300 km and 6,600 km ranges. At night, only ground hop F modes exist except between 8,300 km and 11,600 km, when a chordal F mode may propagate. It should be noted, in this example at least, that the E-F duct potential well is very shallow and in fact is scarcely discernible to the eye. It is also clear that a chordal E mode, while theoretically possible in the daytime, would suffer very high absorption losses in practice.

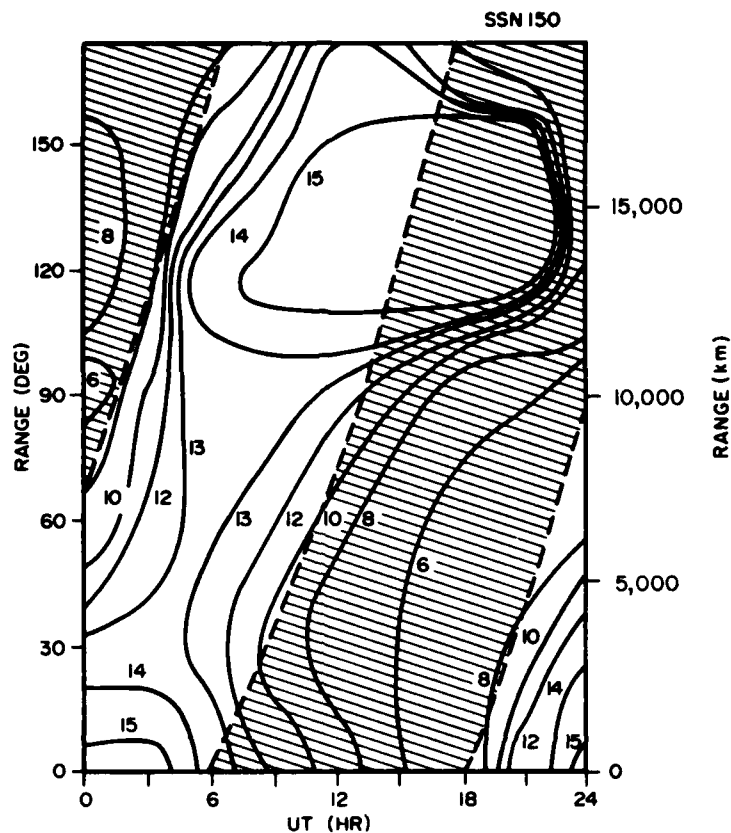


Figure 7. Computed Contours of F-region Critical Frequencies (f_oF_2) Spanned by Distance and Time (UT) for a Particular Propagation Path (SSN = 150)

The altitude range over which ducted propagation is possible is determined by the maximum value (that is, the smallest negative value) of the potential function for the frequency of interest. Figure 13 shows a plot of this maximum value for the E-layer and F-layer boundaries, for selected frequencies (16, 18 and 20 MHz) for UT = 00, SSN = 150. In the free space region below the ionosphere, chordal modes are only possible when $\epsilon < -1$. It is apparent that decreasing the frequency reduces the range over which chordal modes may propagate. In fact at night, in the example illustrated, no chordal F propagation may exist for frequencies less than about 16.5 MHz.

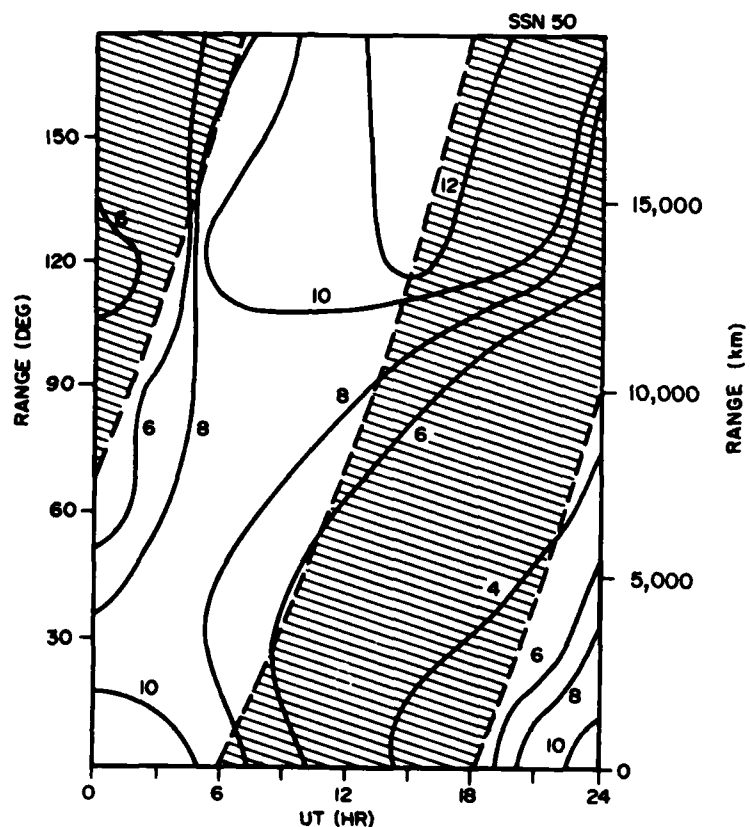


Figure 8. Computed Contours of F-region Critical Frequencies (f_oF_2) Spanned by Distance and Time (UT) for a Particular Propagation Path (SSN = 50)

An estimate of the energy density, which the various ducted modes are capable of supporting along the path, is obtained by computing the adiabatic invariant, defined above. Figure 14 shows $I(f)$ plotted along the direction of propagation for a frequency of 20 MHz. Note the different ordinate scales for the F (chordal) and E/E-F modes, respectively, illustrating the fact that the F-Mode can carry about 20 times more energy than the chordal-E or E-F ducted modes.

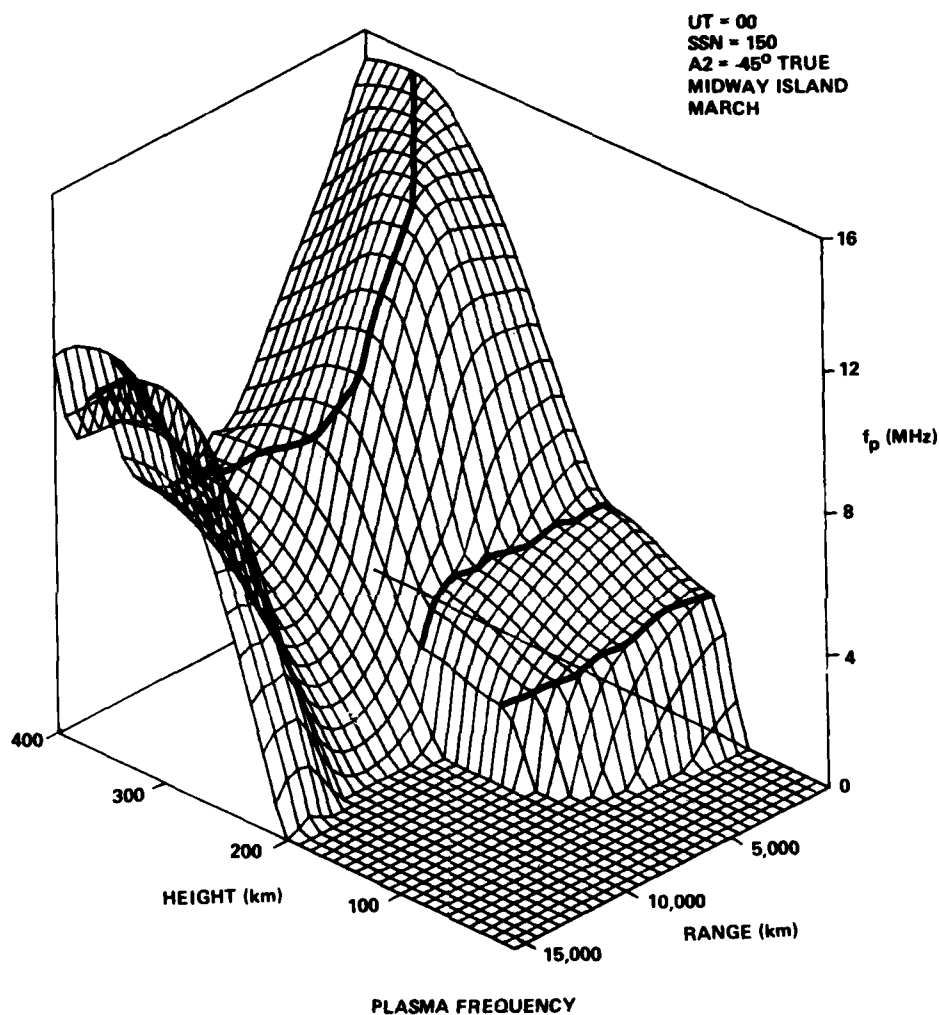


Figure 9. Model Plasma Frequency for Three-layer Ionosphere Varying With Height Above and Range Along a Particular Propagation Path

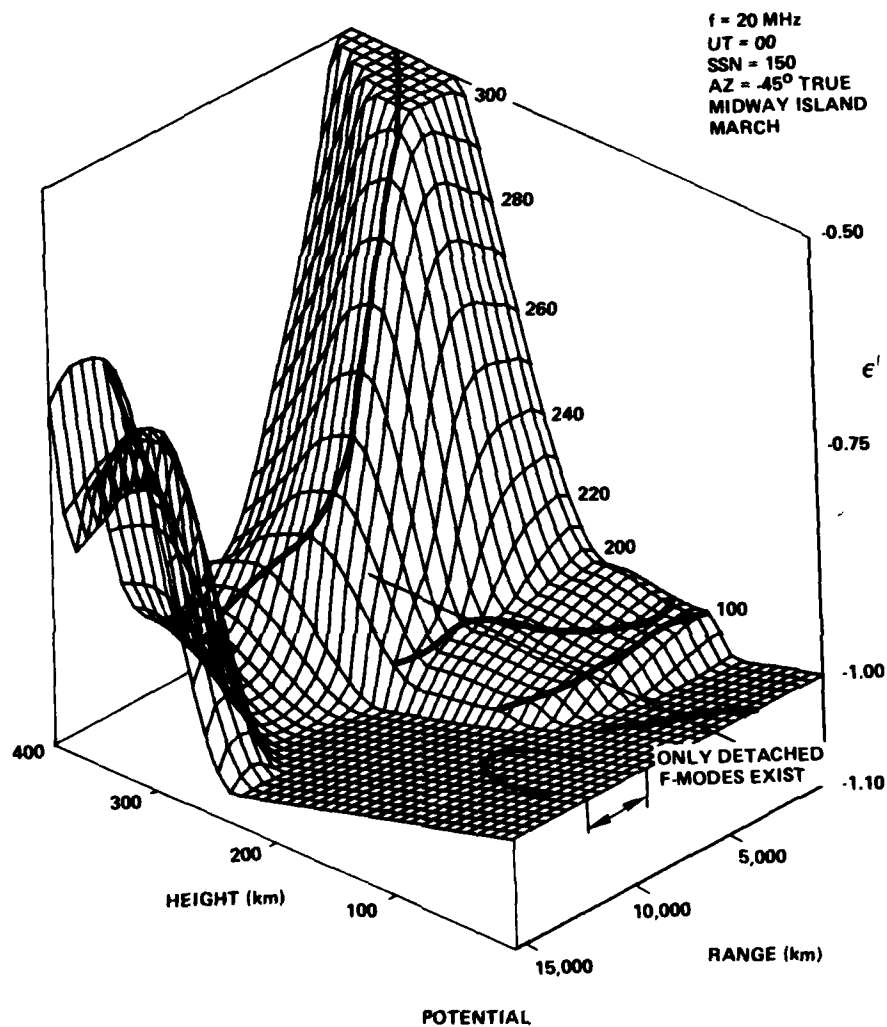


Figure 10. Isometric Display of Potential Function for Ionosphere of Figure 9 Using Operating Frequency of 20 MHz

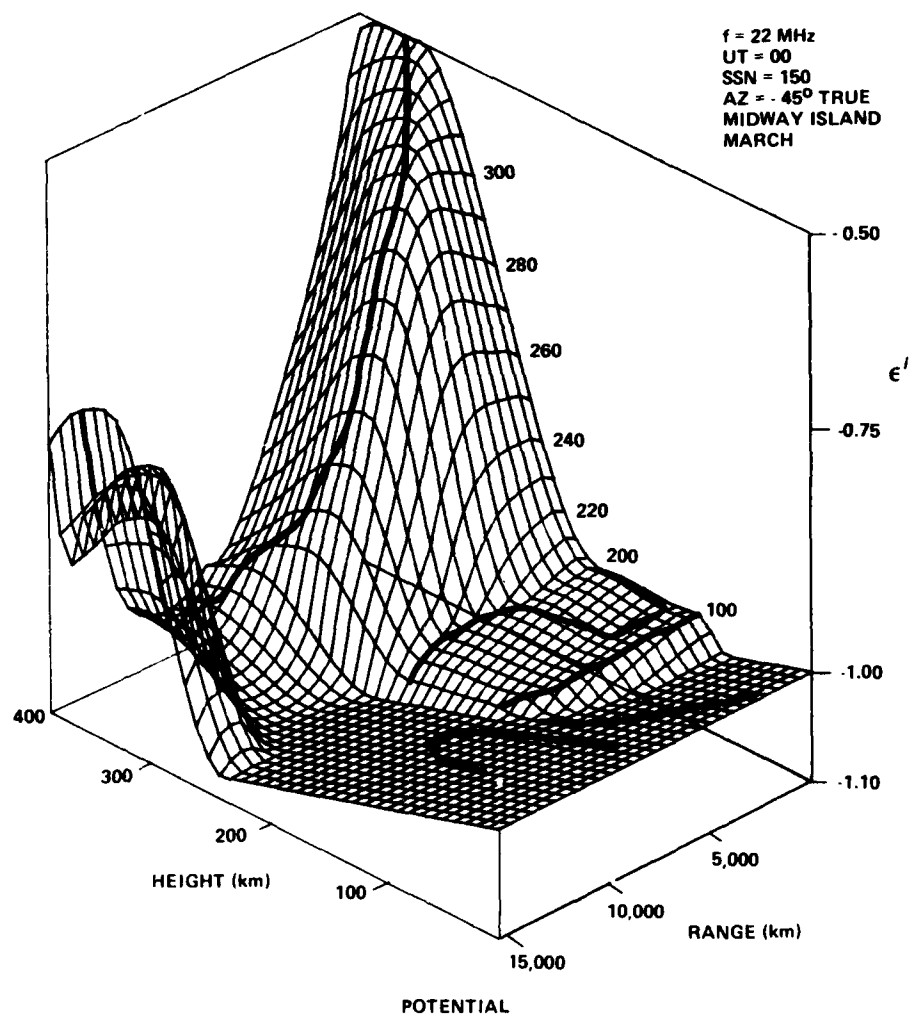


Figure 11. Isometric Display of Potential Function for Ionosphere of Figure 9 Using Operating Frequency of 22 MHz

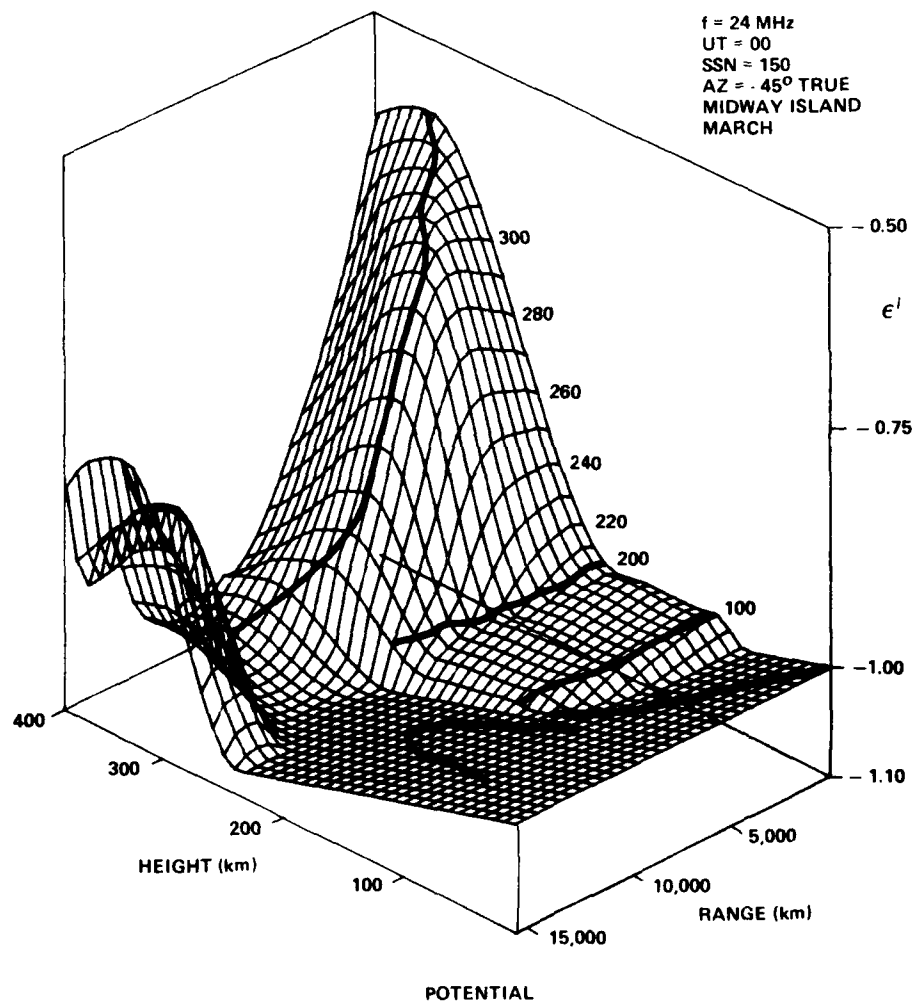


Figure 12. Isometric Display of Potential Function for Ionosphere of Figure 9 Using Operating Frequency of 24 MHz

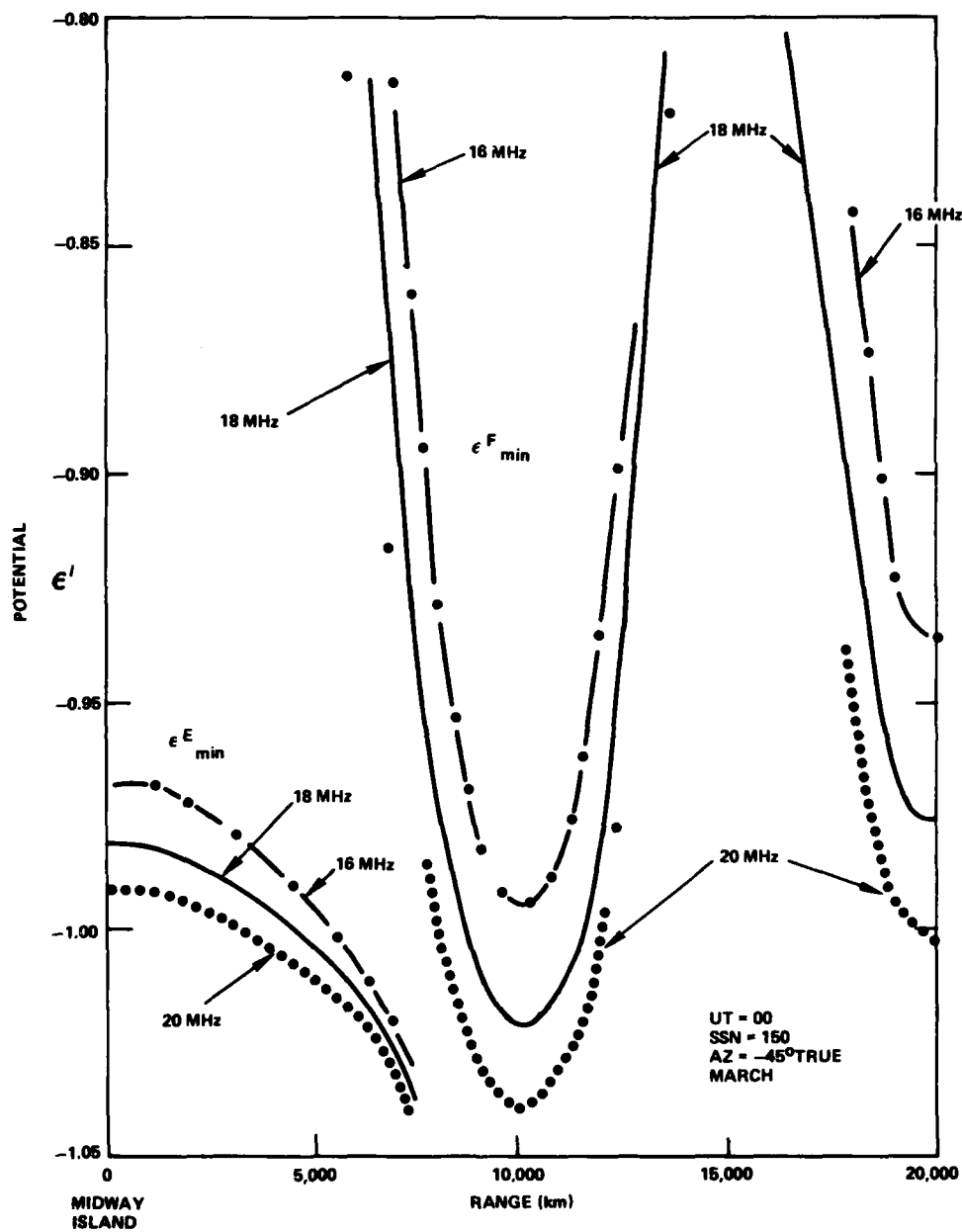


Figure 13. Curves of the Smallest Negative Values of the Potential Function, for E- and F-region at 16, 18, 20 MHz Along the Propagation Path

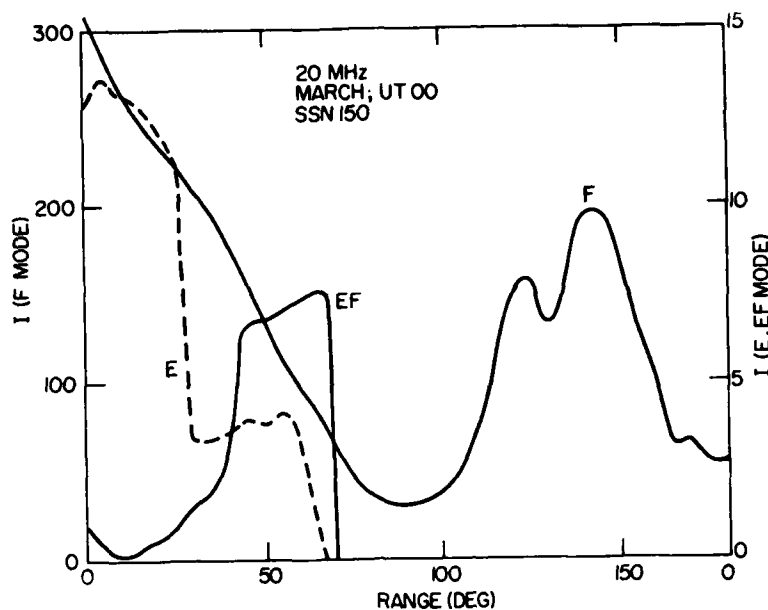


Figure 14. Plots of the Adiabatic Invariant for E, EF and F Mode Varying Along the Propagation Path. (The ordinate scale for the F mode differs from that of the E, EF modes.)

2.3 Coupling to Duct Mode Propagation

In the case of a smooth, spherically stratified ionosphere, it is geometrically impossible for radio energy to be coupled from a ground based source to a ducted propagation mode; chords of the spherical ionospheric cavity which satisfy the reflection condition and intersect the earth's surface at one point (the source) will always intersect the earth at other points as well. In order to couple energy from a ground based source into a ducted mode, some perturbation of the ray trajectory is required at the coupling point. This perturbation may take one of several forms: (1) refraction due to a suitable ionospheric gradient; (2) scattering from natural small-scale irregularities (for example, auroral or equatorial irregularities); (3) scattering from artificially produced ionospheric irregularities (for example, those induced by RF heating, or those accompanying release of suitable chemicals or plasma in the ionosphere, or those produced by electrostatic acceleration of ionospheric electrons). Other possibilities exist, such as a combination of ionospheric gradients and scatter from meteor trails in the lower ionosphere.⁵

5. Vever, A.S., Danilova, T.P., Shlionsky, A.G. (1978) Possibility of the trapping of radio waves, scattered by meteor trails, by ionospheric ducts, Geomagn. Aeron. 18(3):306-308.

2.4 Raytracing Through Natural Gradients

In general, a decreasing electron density gradient in the direction of propagation is required to couple energy from a ground based source into a ducted mode (conversely, an increasing gradient is required for coupling from a ducted mode to a ground based receiver).² Suitable gradients exist under commonly occurring situations, such as crossing the solar terminator (day-night boundary in the ionosphere), propagation through the polar and equatorial regions, and traveling ionospheric disturbances. The frequency range and the range of elevation angles, over which trapping in ducts may take place, are functions of the magnitude of the gradient and of the location of the irregularity relative to the source on the ground.

Computations have been performed, using models of the ionosphere, together with numerical raytracing procedures, to establish the range of frequencies and elevation angles over which ducting can occur in typical cases. An example of such a computation is presented here in which the influence of strong gradients near sunset is considered.

A transmitter was assumed to be directing radio energy at low elevation angles, from a location at latitude 32° in a northeasterly direction. The ionosphere was modeled along the direction of propagation at 1415, 1515, 1615 and 1715 LT at the transmitter, for the month of October, at sunspot number 100. Figure 15 shows the location of the evening solar terminator, at these four times, relative to the transmitter and direction of propagation. It is seen that at 1415 the entire ionospheric propagation path is in sunlight, while at 1715 it is in darkness. At 1515 and 1615 LT, large gradients are modeled along the propagation path.

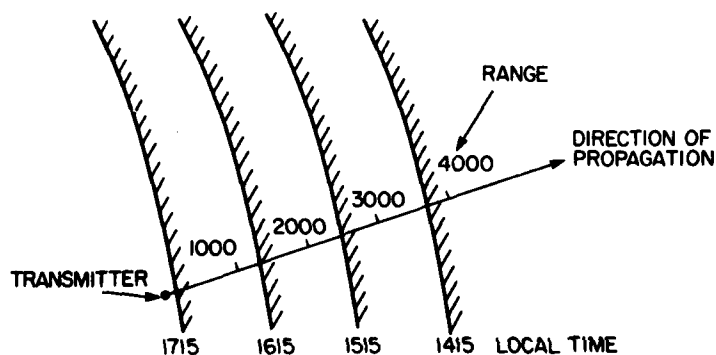


Figure 15. Progression of Solar Terminator Toward Transmitter

Three dimensional numerical raytracing was performed at a frequency of 30 MHz in the four modeled ionospheres, with the results depicted in Figure 16 where the top panel corresponds to 1415 LT and time progresses downwards to 1715 in the bottom panel. Each panel shows an elevation cut and an azimuthal cut through the fan of rays from 0° to 10° in steps of 1° in elevation. The lower part of each panel shows the elevation cross section relative to the surface of the earth, while the upper part shows the azimuthal cross section relative to the propagation direction. Range is indicated by the scale graduated in units of 500 km (the first 500 km is subdivided into 100 km steps).

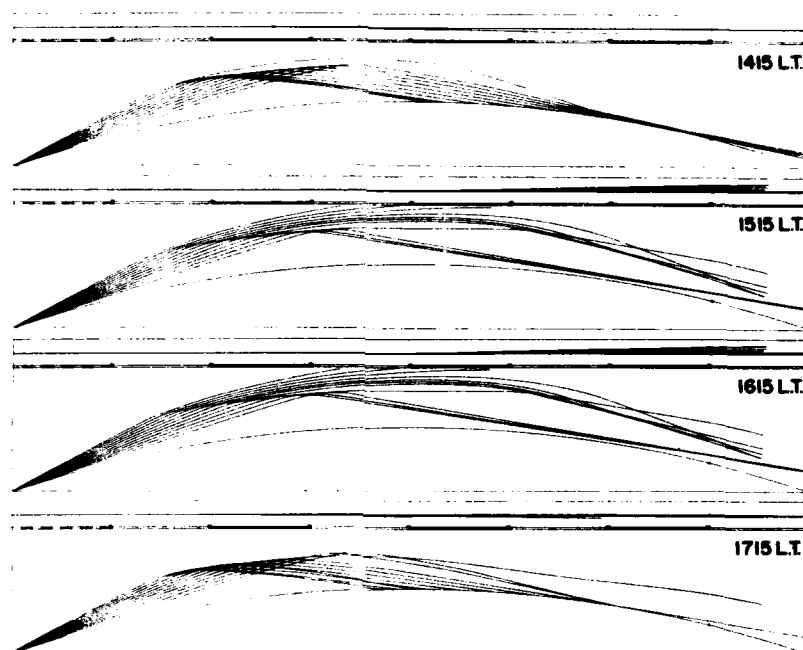


Figure 16. Sequence of Three-dimensional Numerical Raytracings Through Model Ionosphere at Four Local Times for a Fixed Transmitter

The daytime and nighttime ionospheres display essentially classical hop type propagation (note that the ray plots are terminated when the ray intersect the earth). At 1715 (night), however, one ray is apparently ducted and a second just grazes the earth. The intermediate ionospheres support injection of the entire transmitted rays into chordal and ducted modes, as a result of the large negative electron density gradients along the direction of propagation.

2.5 Scattering from Irregularities

The phenomenon of scattering of radio waves from ionospheric small-scale irregularities is essentially the same for both naturally occurring and artificially produced irregularities. The only practical differences lie in the possibly different scale-size spectra and different spatial extents involved in the two cases.

Figure 17 illustrates the geometry involved when radio waves of power density P_0 are incident on elongated irregularities at angle χ . The power scattered into an element of solid angle, $d\Omega$, at angle ψ to the irregularity axis, from an incremental element of scatterer volume, dV , is

$$dP_s = P_0 \sigma(\theta) d\Omega dV$$

where θ is the scattering angle, that is, the angle between incident and scattered vectors and $\sigma(\theta)$ is the "volumetric scatter cross section," that is, the equivalent point target cross section per unit volume of scatterers. In the ionosphere, the scatterers are elongated along the direction of the local magnetic field; the volumetric cross section is a strong function of the scatter angle θ .

The equivalent point target cross section of a finite volume V_s of scatterers is

$$\sigma_s(\theta) = \int_{V_s} \sigma(\theta) dV$$

Erukhimov et al⁶ have given the formula for the volumetric, cross section of long, thin plasma irregularities having a Gaussian electron density distribution, for the general case of arbitrary angles of incidence and scatter. Taking their results and making minor changes in symbols, we obtain

$$\sigma(\theta, \gamma) = \frac{k^4 \eta l^3}{16\sqrt{\pi}} \langle (\Delta\epsilon)^2 \rangle \cdot \exp - (k\eta l \sin \frac{\theta}{2})^2 \cdot (\cos^2 \gamma + \frac{1}{2} \sin^2 \gamma)$$

where

$$k = 2\pi/\lambda$$

$$\lambda = \text{wavelength}$$

6. Erukhimov, L.M., Matyugin, S.N., Uryadov, V.P. (1975) Radio wave propagation in ionospheric wave channels, Radiophysics & Quantum Electronics 18(9):958-963.

l = scale size transverse to the magnetic field

$\langle(\Delta\epsilon)^2\rangle$ = mean square fluctuation of dielectric constant corresponding to scale size l

η = ratio of irregularity dimensions parallel and transverse to the magnetic field

$$\cos \gamma = \frac{\cos \psi - \cos \chi}{2 \sin \frac{\theta}{2}}$$

Note that

$$\langle(\Delta\epsilon)^2\rangle = \frac{\omega_o^4}{\omega^4} \left(\frac{\Delta N}{N} \right)^2$$

where

ω_o = local plasma frequency

$\omega = 2\pi c/\lambda$ = frequency in radians

c = velocity of light

N = electron density of background plasma

ΔN = rms electron density fluctuation

The expression for volumetric cross section may be written⁶ in the useful form

$$\sigma(\theta, \psi, \chi) = \frac{\kappa^4 \eta l^3}{16\sqrt{\pi}} \left(\frac{\Delta N}{N} \right)^2 \frac{\omega_o^4}{\omega^4} \cdot \exp(-\kappa^2 l^2) \cdot \left[\frac{1}{4} (\eta^2 - 1) \cdot (\cos \psi - \cos \chi)^2 + \sin^2 \frac{\theta}{2} \right]$$

There are two important special cases of the formula for volumetric cross section. (1) Scattering cone: When $\psi = \chi$, the first term in the exponential factor is zero, corresponding to a maximum in cross section. This is the so-called specular reflection condition, and is satisfied on the surface of a cone whose axis is the axis of the irregularity. (2) Forward scatter: When $\theta = 0$, the second factor in the exponential term is zero, corresponding to a maximum in cross section.

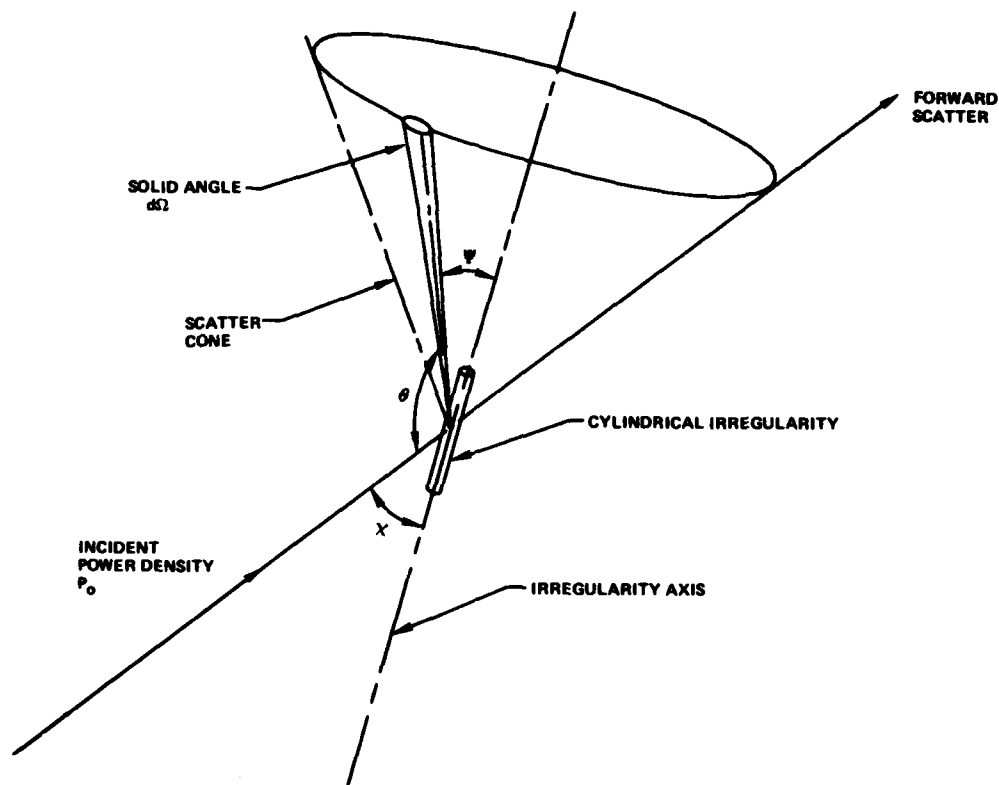


Figure 17. Scattering Geometry for Reradiation of Incident Electromagnetic Waves by Elongated Irregularities

An interesting special case is that in which the incident and scattered vectors are both in the magnetic meridian plane, in which case

$$\theta = \psi - \chi$$

and the volumetric cross section is a function of ψ and χ alone.

Figures 18 and 19 illustrate the variation in reflected power (normalized to unit incident power) as a function of scatter angle θ for ranges of values of the transverse irregularity dimension and anisotropy. Figure 20 illustrates the aspect sensitivity of the scatter for the same ranges of parameters, as a function of wavelength, close to orthogonality. [Note that the curve for $(l = 100, \eta = 20)$ coincides almost exactly with that for $(l = 300, \eta = 10)$.] It is apparent that the aspect sensitivity of the scatter increases as irregularity size and anisotropy increase (for a given wavelength) or wavelength decreases (for given irregularity dimensions).

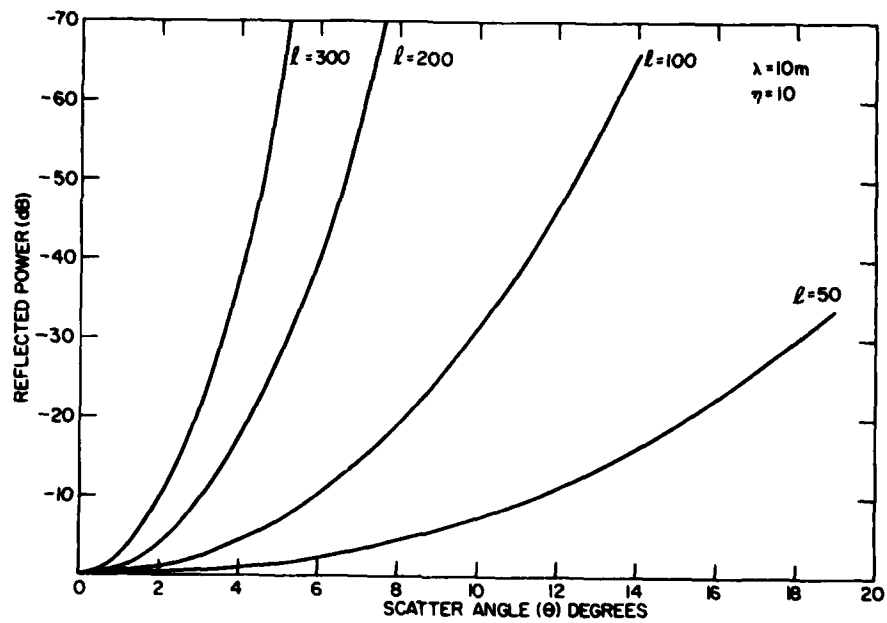


Figure 18. Normalized Reradiated Power as a Function of Scatter Angle for Ranges of Transverse Irregularity Dimension l and Anisotropy η ($\lambda = 10\text{ m}$)

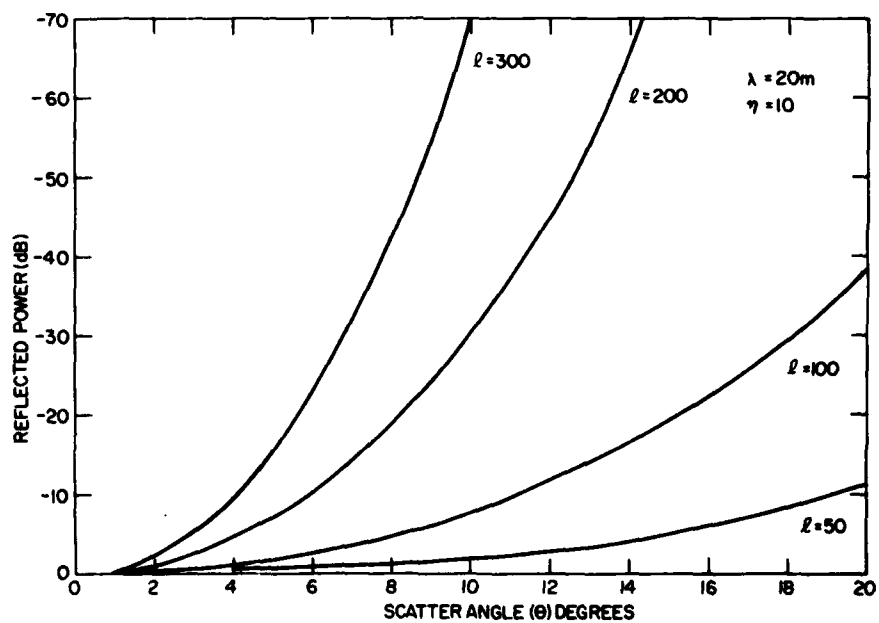


Figure 19. Normalized Reradiated Power as a Function of Scatter Angle for Ranges of Transverse Irregularity Dimension l and Anisotropy η ($\lambda = 20\text{ m}$)

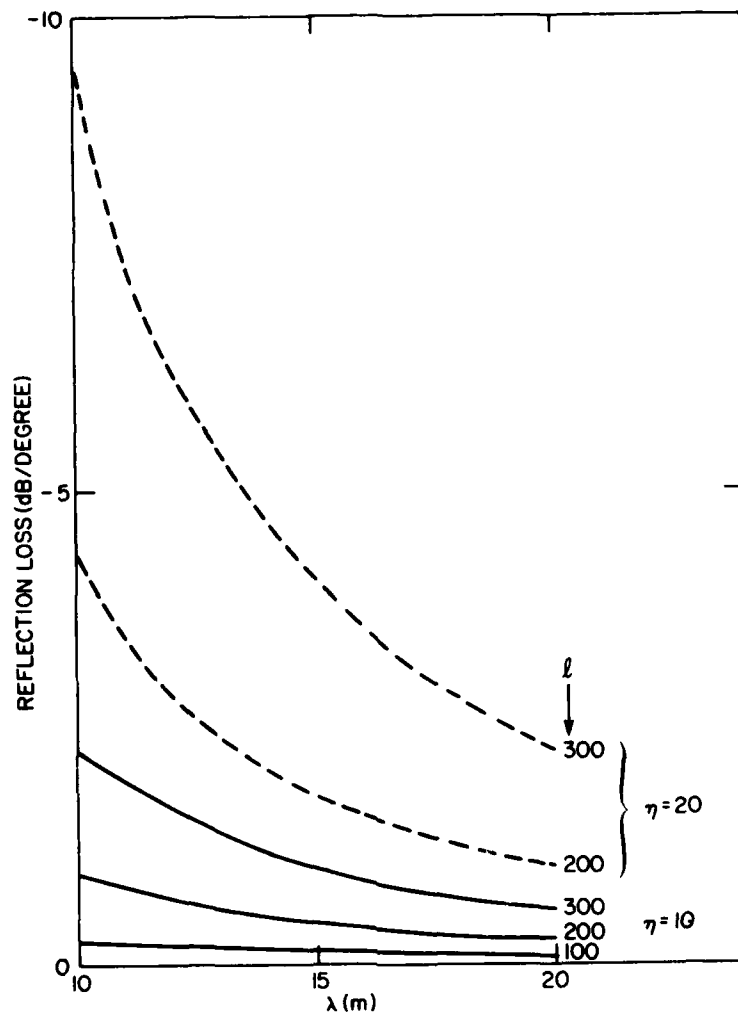


Figure 20. Computed Wavelength Dependence of Aspect Sensitivity Near Orthogonality ($\theta \rightarrow 0$)

2.5.1 SCATTERING AT HIGH FREQUENCIES

At frequencies well above ω_o , the plasma frequency, the refraction of incident and scattered waves is small, and straight line propagation geometry is a reasonably accurate approximation. If attention is also confined, for simplicity, to propagation in the magnetic meridian plane, ψ is the local magnetic inclination for ducted waves traveling horizontally.

2.5.2 SCATTER GEOMETRY WITH RADIO WAVE REFRACTION

The field-aligned scatter, which can act as a means of coupling energy in and out of ionospheric ducts, has thus far been considered only in the high frequency limit, that is, with consideration of radio refraction neglected. In fact, for radio frequencies in the HF band, considerable refraction is encountered in the radio path through the ionosphere below the scattering region, especially at the low end of the band and in the daytime. Thus the straight-line propagation geometry must be modified to reflect the actual propagation conditions, which is a task of considerable complexity.

Computations have been performed in which the ionosphere was modeled in three dimensions, using a general purpose model,⁷ and rays were traced appropriately through this model over a range of frequencies. A ducted mode was assumed to be propagating towards the scattering point from one of several azimuths (0° to 360° in 45° increments); after specular scattering and refracted propagation through the lower ionosphere, the points of intersection of the rays with the earth's surface were computed. In order to permit some deviation from a rigid requirement for horizontal propagation in the ducted wave, the angle of incidence upon the scattering point was assumed to take the values 0° , $\pm 5^\circ$ with respect to the horizontal at that location. This permitted some estimate to be made of the ground locus of intersection within a 10 degree range of angles for the ducted wave vector. (See Section 3.2, Figure 33.)

2.6 Propagation Loss Evaluation

In order to estimate the absorption losses for radio waves trapped in ionospheric ducts, a propagation analysis was conducted in which a numerical ionospheric model was constructed and rays subsequently traced in this model. The modeling and raytracing procedure which was used permitted the computation of absorption due to both electron-neutral and electron-ion collisions.⁷ Radio waves propagating in the F-region are influenced relatively little by electron-neutral collisions, due to the relatively low concentration of neutral atoms at F-region altitudes; the major contribution to absorption at these altitudes comes from electron-ion collisions.

A source of radio energy, in the frequency range 10 to 21 MHz was assumed to exist at several altitudes in the ionosphere, and propagation to a range of 10,000 km was considered. The elevation angle of the initial ray vector at the

7. Rush, C.M., Elkins, T.J. (1975) An assessment of the magnitude of the F-region absorption on HF radio waves using realistic electron density and collision frequency models, ITU Telecommunication Journal, Geneva.

source was varied over a wide range and this angle, together with the ionospheric structure along the path, determined the propagation mode. Figure 21 shows the results of the attenuation calculations for four values of the source altitude between 110 and 170 km. Also illustrated are two possible propagation modes — one classical hop-type and one ducted (chordal). The general trend in the dependence of attenuation on frequency reflects the approximate inverse-square dependence which is well-known from classical theory. There is also a pronounced inverse dependence upon the altitude of the source, which reflects the larger proportions of the propagation paths in the lower regions of the ionosphere for lower source altitudes. For the 170-km source altitude, a group of points is found to exhibit extremely low absorption in the frequency range 15 to 20 MHz, as indicated by the dashed contour. These correspond to ducted modes, for which the absorption losses are in the range 2 ~ 4 dB for the 10,000-km path.

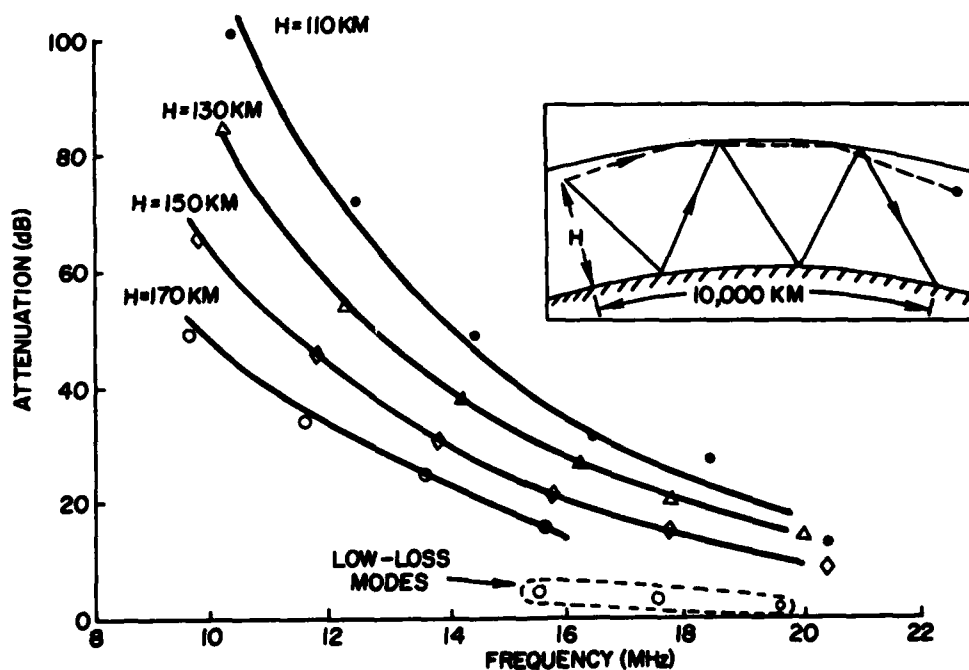


Figure 21. Sample Illustration of Propagation Loss, Computed for Different Transmitter Heights, Over a 10,000-km Propagation Path

3. GROUND-BASED PROPAGATION EXPERIMENTS

3.1 Round-the-World (RTW) Propagation

High frequency waves which travel completely round the world (so-called RTW propagation) may be taken as evidence of the existence of ionospheric ducting over appreciable portions of the path; otherwise lower ionospheric absorption in the sunlit hemisphere would have reduced their signal strength below the level of detectability. A related indication of ducting is the propagation of significantly large energy along the long portion of the great circle joining two relatively close points (so-called "back-path" propagation). Round-the-world propagation has been studied for many years,⁸ but a consistent explanation of the phenomenon has only recently emerged.⁹ Based on theoretical and experimental considerations, it is apparent that the optimum conditions for RTW propagation are along a great circle which is close to the solar terminator (the twilight line). Generally speaking, the greater the angular separation between the propagation path and the optimum RTW great circle, which itself is displaced 15° to 20° from the terminator, the less favorable are conditions for RTW propagation.

A number of RTW and related experiments have been conducted to investigate the ducting phenomenon. An FM/CW transmitter, operating at 1-kW power in the frequency range 6 to 30 MHz was coupled to a horizontally polarized log periodic antenna (gain ~ 14 dB relative to isotropic) directed northwards from Ava, New York (lat. 45°). The receiving antenna, located at nearby Verona, New York consisted of an array of Beverage elements having a mid-band gain of about 12 dB, directed south. Swept frequency ionograms were recorded around the clock at 20 min intervals, with RTW propagation being frequently observed. Figure 22 shows an example of such an ionogram; note the diffuse nature of the trace and the bifurcation at the high frequency end, a characteristic feature of these RTW measurements. The maximum and minimum observed frequencies were extracted from a sample eight hour period of ionograms and are plotted in Figure 23 together with the observed group delay. Also shown are the time of sunrise at the approximate latitude of the ionospheric entry point (55°) and at the equator of the longitude of the transmitter/receiver pair. Note the approximate symmetry of the period of RTW observation about 12 UT, that is, along the optimum RTW great circle.⁹ The group path, measured at the time of arrival of the earliest signal returns (the leading edge) shows a maximum variation of about 0.5 msec

8. Toman, K. (1979) High-frequency ionospheric ducting - A review, Radio Science 14(3):447-453.

9. Golyan, S. F. (1975) Optimal conditions for extra-long-range short-wave propagation, Radiophysics & Quantum Electronics 18(9):1014-1022.

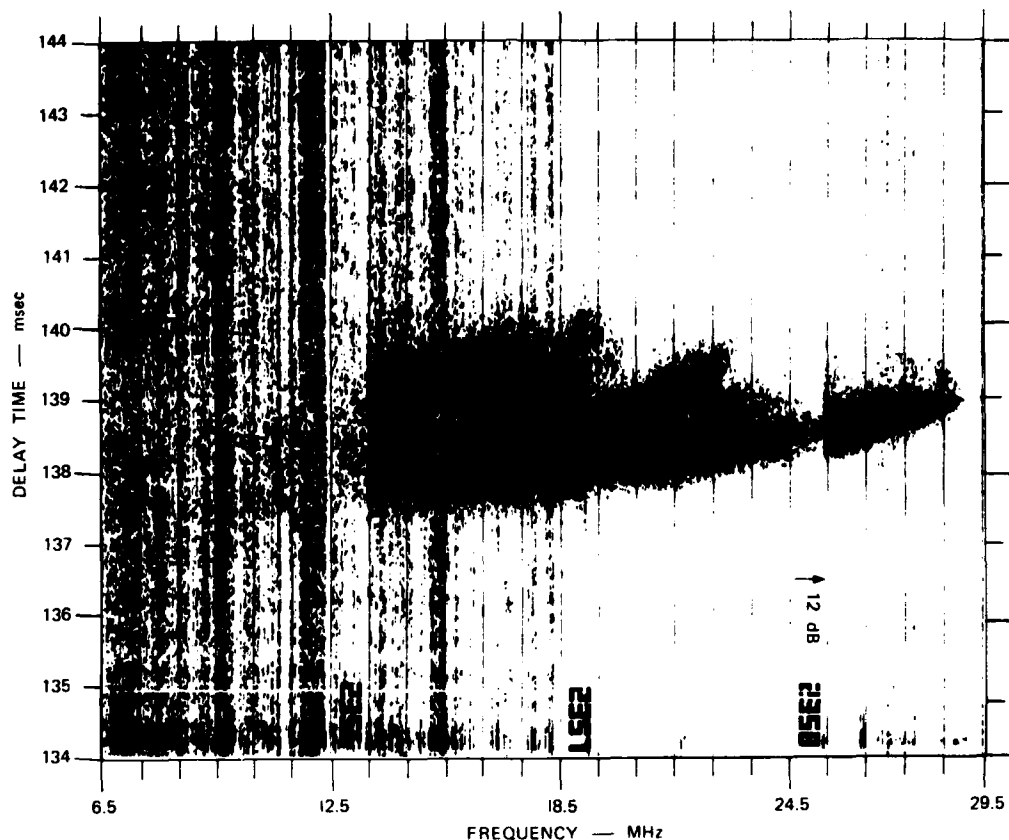


Figure 22. Round-the-world Echo of FM/CW Signal Radiated Northward From Ava, NY and Received at Verona, NY About 137.5 msec later

(150 km) over the observing period. Since the longer group paths are associated with the highest values of the minimum observed frequency, it is presumed that the propagation path involved more ground reflections, resulting in higher absorption, during the period ~11 to 14 UT than in the earlier part of the observed RTW period.

A second type of measurement was made in which transmissions from Ava were directed both towards the east and towards the west, with reception at Los Alamos, New Mexico. The Platteville heating facility, operated by the Institute for Telecommunications Sciences, Boulder, Colorado, was used to modify the ionosphere with its ten 200 kW transmitters, feeding a circular array of broadband dipoles that can tune from 5 to 10 MHz. With an antenna gain of

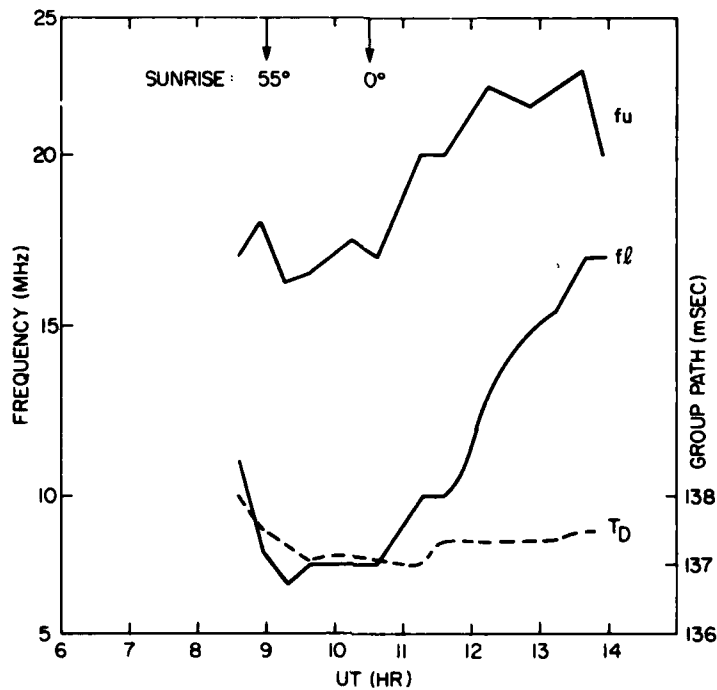


Figure 23. Observed Maximum and Minimum Frequencies in Megahertz of Round-the-world Echoes and Their Group Delays in Milliseconds

20 dBi and a half-power beamwidth of 16 degrees at 7.5 MHz the heater could modify a $400 \times 400 \times 20$ (altitude) km volume. It was of interest to determine whether the Platteville heater was operating during this period, and the intent was to determine whether or not radio energy could be scattered from an ionospheric duct forming a part of the RTW propagation path.

Figures 24 and 25 illustrate two examples of quasi-RTW propagation. In the first example, Ava is transmitting towards the east so that the energy is propagating along the "back-path"; in the second example, Ava is transmitting west, and the received radio energy has propagated slightly longer than one transit around the earth. These two examples were selected to show two different types of RTW—the first exhibiting substantial multipath (that is, several relatively discrete modes) whereas the second is more intense and has a sharply defined leading edge with diffuse trailing edge. During both of the measurements illustrated here, the ionospheric heater/modifier was off.

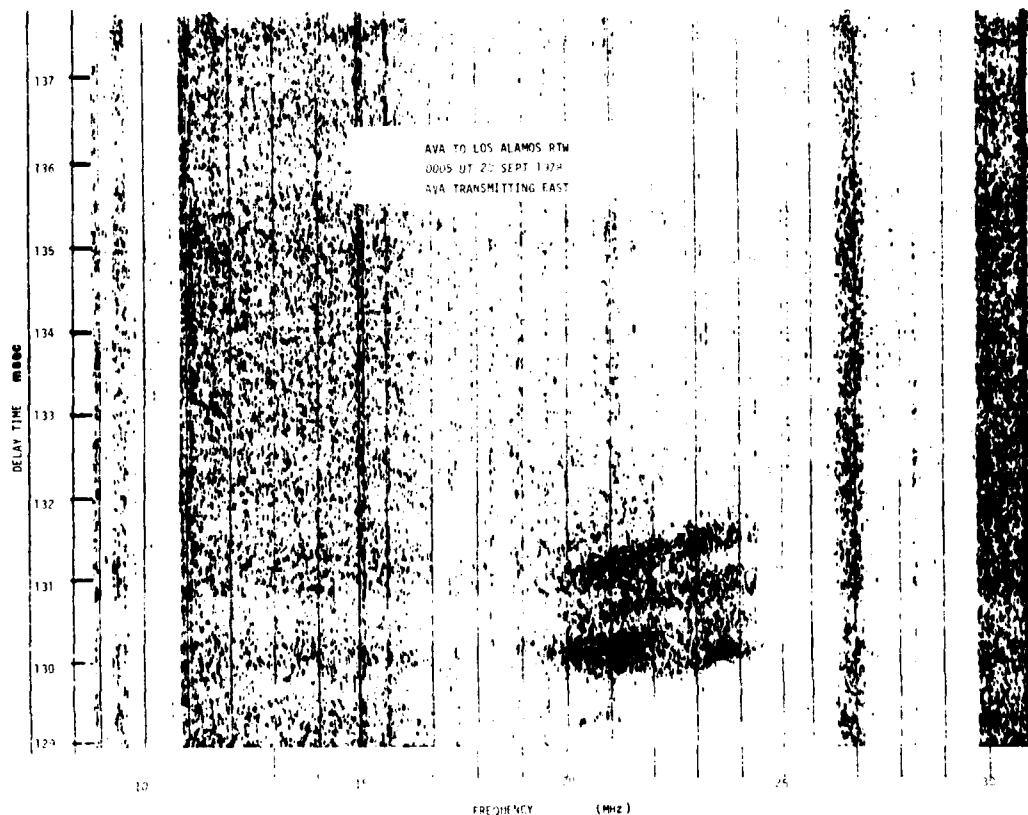


Figure 24. Round-the-world Echo of FM/CW Signal Radiated Eastward from Ava, NY and Received at Los Alamos, New Mexico

Figures 26 to 30 show examples of data sets in which the heater was cycled on and off at 5-min intervals or longer (indicated by the binary vertical markers along the abscissas). Again plotted are the upper and lower observed RTW frequencies and the group delay. Most of these data were collected near the autumnal equinox and Figure 31 shows the distribution of observed RTW periods, grouping around sunset (~ 00 UT) and sunrise (~ 14 UT). Figure 30 shows summer data, with RTW echoes centered around sunset (~ 02 UT). Also shown in Figure 30, for comparison purposes, is the maximum observed frequency (MUF) propagating over the direct path from Ava to Los Alamos, indicating that the maximum RTW frequency was only 1 to 2 MHz higher than the classical MUF for most of the observing period. It appears from the data in Figures 26 to 30

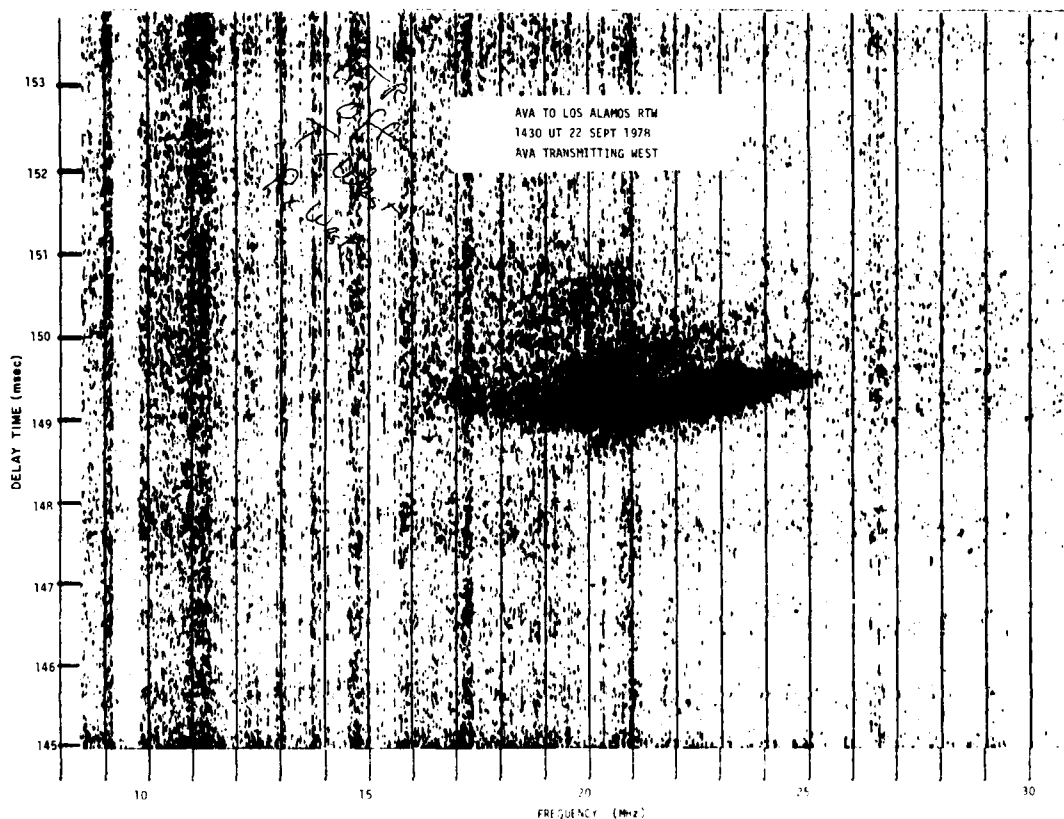


Figure 25. Round-the-world Echo of FM/CW Signal Radiated Westward From Ava, NY and Received at Los Alamos, New Mexico

that the presence of heater-generated ionospheric irregularities has no discernible effect on the range of frequencies propagating in the RTW signal. Qualitative examination of the data reveals that the heater also has no apparent effect on the intensity of the RTW signals.

The observation that heating of the ionosphere had no apparent effect on the RTW signal has at least two possible interpretations: (1) The scatter cross section of the heater-produced irregularity cloud was sufficiently small that any additional energy scattered from the RTW signal was below the noise level; this is not unreasonable since the measured RTW levels were very close to noise level. (2) The irregularity cloud was too high in the ionosphere with the result that the heater-induced scatterers were outside the range of altitudes in which the ducted signal was propagating.

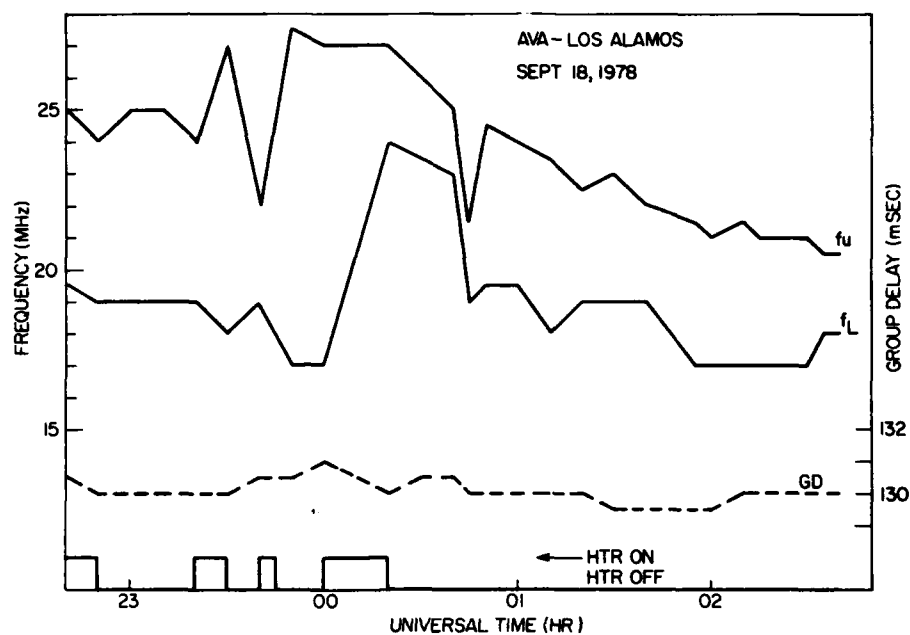


Figure 26. Sep 18, 1978, Ava - Los Alamos, Observed Maximum and Minimum Frequencies in Megahertz of Round-the-world Echoes and Their Group Delays in Milliseconds

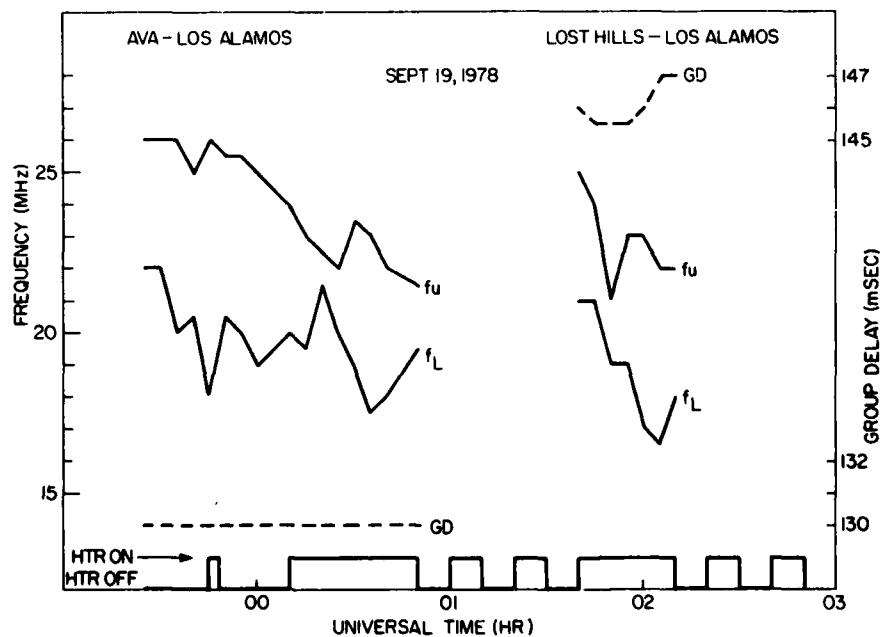


Figure 27. Sep 19, 1978, Ava - Los Alamos, Lost Hills - Los Alamos, Observed Maximum and Minimum Frequencies in Megahertz of Round-the-world Echoes and Their Group Delays in Milliseconds

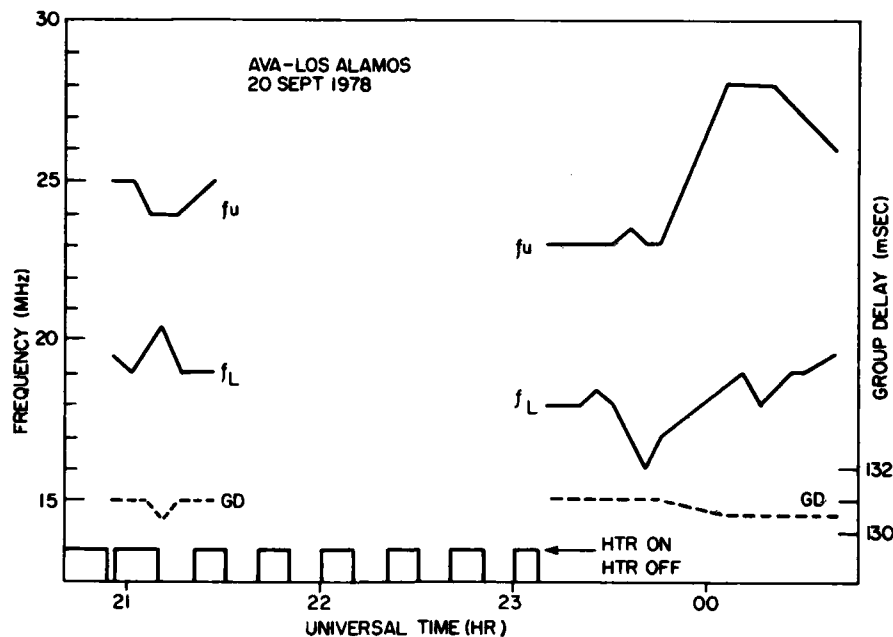


Figure 28. Sep 20, 1978, Ava - Los Alamos, Observed Maximum and Minimum Frequencies in Megahertz of Round-the-world Echoes and Their Group Delays in Milliseconds

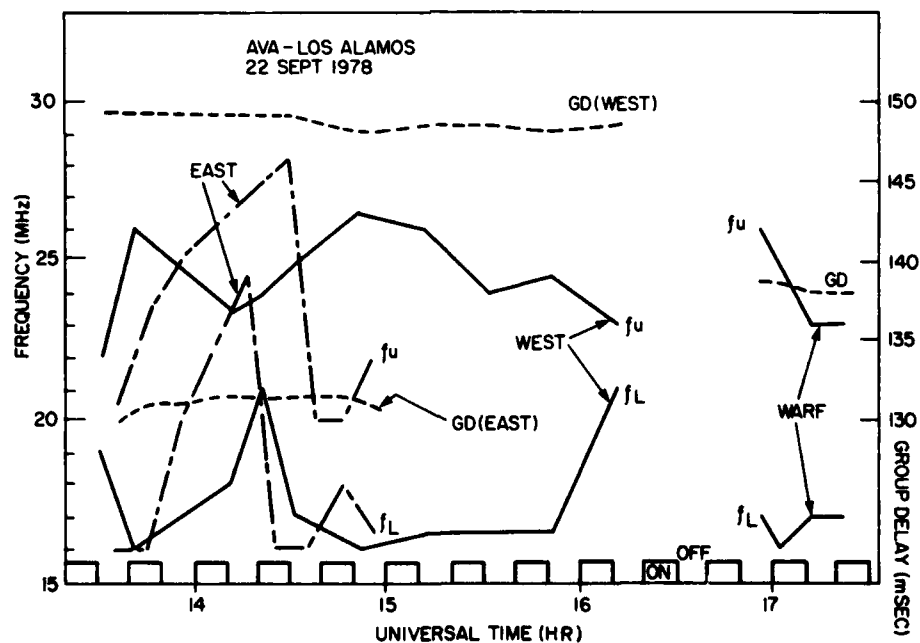


Figure 29. Sep 22, 1978, Ava - Los Alamos, Observed Maximum and Minimum Frequencies in Megahertz of Round-the-world Echoes and Their Group Delays in Milliseconds

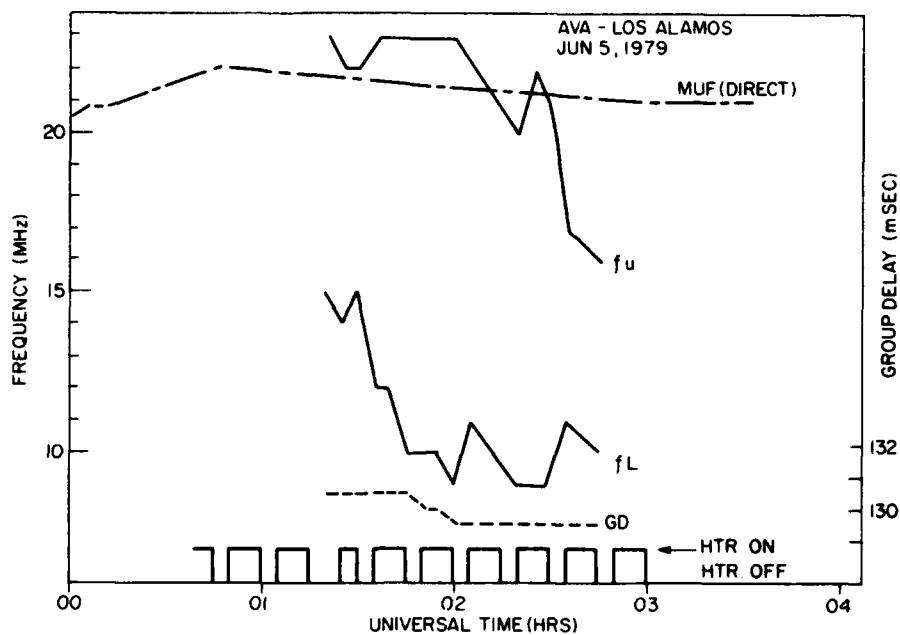


Figure 30. June 5, 1979, Ava - Los Alamos, Observed Maximum and Minimum Frequencies in Megahertz of Round-the-world Echoes and Their Group Delays in Milliseconds

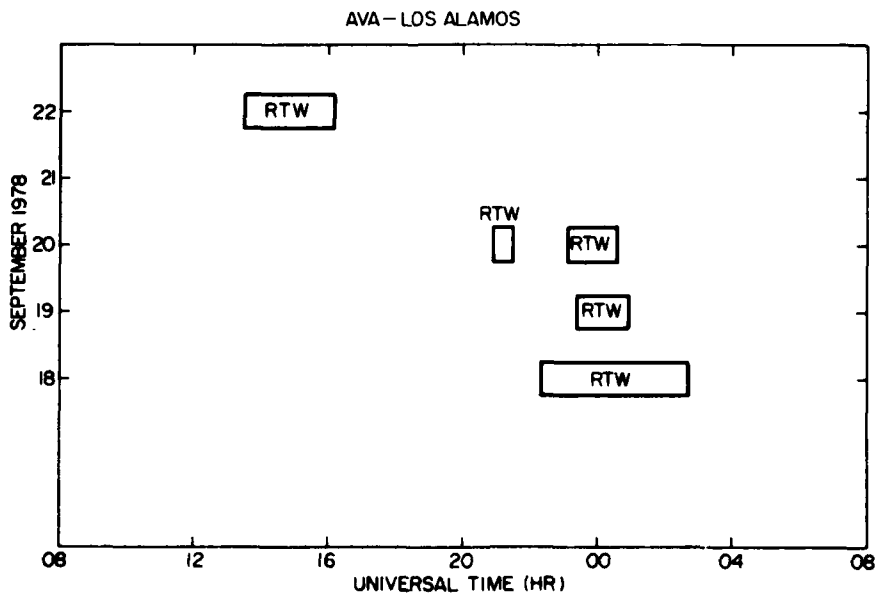


Figure 31. Preferred Times of Occurrence of Round-the-world Echoes Between Ava, New York and Los Alamos, New Mexico from 18 to 22 Sep 1978

The second possibility is regarded as being the more likely one since the lower frequency limit of the heater (5 MHz) was close to the maximum F-region plasma frequency for much of the nighttime observing periods. Thus heating was taking place mostly above about 250 km, and RF energy propagating in the chordal mode (the dominant ducting mode at night) can be expected to travel at a lower altitude than this value.

3.2 Long-range Propagation

Several ducted-propagation experiments have been conducted between 1978 and 1980 which involved the ionospheric radio-frequency heating facility at Platteville, Colorado, operated by the Institute for Telecommunications Sciences, Boulder, Colorado. This radio-frequency heating facility was used to create in the F-region a heater cloud whose fine structure contained field-aligned ionization irregularities. These irregularities were expected to scatter incoming high-frequency signals, originating from remote transmitting sites, to receiving sites whose general location relative to Platteville was deduced from the geometry provided by ionization irregularities.

Characteristics of the geometry were: (1) Irregularities are constrained to be aligned with the orientation of the local geomagnetic field, (2) irregularities occur at heights that depend on the height distribution of the ambient ionosphere plasma frequency and the heater frequency, (3) Direction of the incident radiation originating from remote ground-based transmitters.

Transmitting and receiving sites used in the experiments, along with surface distances and propagation delay between stations are illustrated in Figure 32. Table 1 gives the location of participating stations, transmitter power, antenna gain, and range of operating frequencies.

The sounding transmissions from the Stanford Research Institute, International facility at Lost Hills, California, from the RADC facility at Ava, New York, and from the Australian site at Adelaide employed a linear swept-frequency continuous wave (SFCW) system. These transmissions were directed toward Platteville, Colorado, where the RF heater transmitter was operated by the Institute for Telecommunications Sciences. The most notable effect of the heating process is the creation of ionospheric irregularities in the F region by the heater beam. The artificially created irregularities within the heated volume are aligned in the direction of the earth's magnetic field. A receiving station located at Los Banos, California obtained, for the Lost Hills transmission, backscatter information on the cross section of the irregularity volume over Platteville, as well as ground backscatter by way of ionospheric reflections. The receiving stations at Los Alamos, New Mexico and Alamosa, Colorado, were selected on

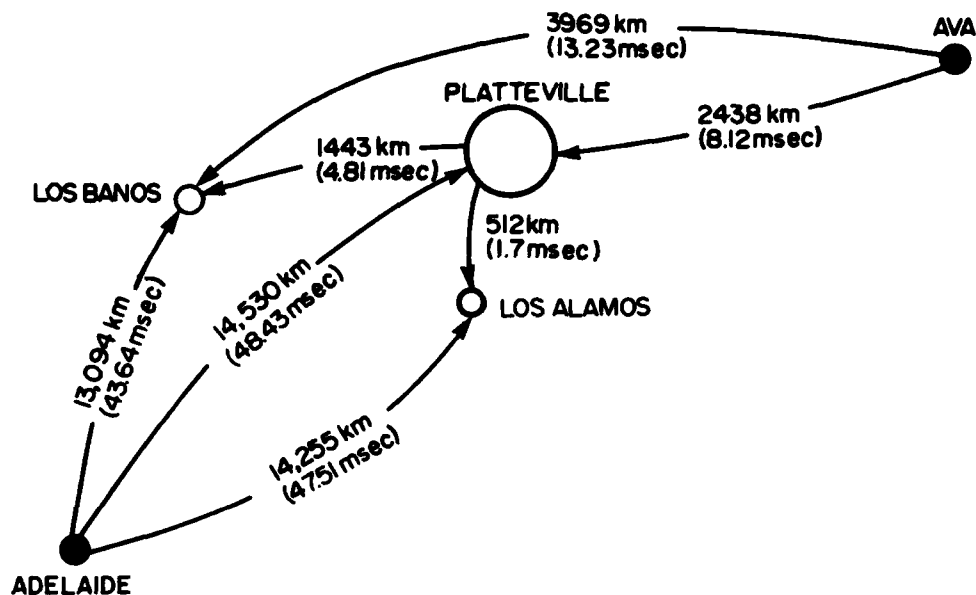


Figure 32. Layout for High-Frequency Propagation Experiment Utilizing the Ionospheric Heater. (Units for surface distance and transmission delay are kilometer and millisecond; solid points represent transmitters; open points represent receiving stations.)

Table 1. Participating Transmitting and Receiving Stations

| Location | Latitude | Longitude | Transmitter Power (kW) | Antenna Gain (dBi) | Frequency (MHz) |
|------------------------|----------|-----------|------------------------|--------------------|-----------------|
| Platteville, Colorado | 40.2°N | 104.7°W | 1500 | 20 | 5-10 |
| Adelaide, Australia | 34.85°N | 138.66°E | 10 | 20 | 6-30 |
| Los Banos, California | 37.06°N | 120.83°W | - | 28 | 6-30 |
| Lost Hills, California | 35.8°N | 120°W | 20 | 18 | 6-28 |
| Alamosa, Colorado | 37.43°N | 105.86°W | - | 10 | 6-30 |
| Los Alamos, New Mexico | 35.76°N | 106.23°W | - | 10 | 6-30 |
| Los Lunas, New Mexico | 34.82° | 106.74°W | 0.3 | 16 | 6-30 |
| Ava, New York | 43°N | 75.5°W | 10 | 16 | 6-30 |

the basis of computations of the family of scattering cones, of field-aligned irregularities, that intersect the surface of the earth at loci which depend on the chosen geomagnetic field model, arrival angle of the electromagnetic wave relative to magnetic azimuth and elevation angle incident at the irregularity, the height of the irregularity, and sounding frequency because of frequency-dependent refraction effects in the ionosphere.¹⁰

Figure 33 illustrates the results of sample calculations of loci resulting from the intersection of scattering cones, associated with field-aligned irregularities, with the surface of the earth, refraction in the ionosphere included. The conditions derived from an ionospheric model are typical of autumn, noon, sunspot number 150. The origin of the scattering cones are placed at a height of 200 km. At that height above Platteville (P), Colorado (lat. 40.2°N , long. 104.7°W ; see Table 1) electromagnetic signals were allowed to arrive at elevation angles of 0° , $+5^{\circ}$, -5° . In Figure 33, this angle was $+5^{\circ}$ above the horizontal at a height of 200 km over Platteville.

Signal frequencies of 6, 12, 18, 24 and 30 MHz were used to compute rays that are specularly reflected from field-aligned irregularities, each frequency resulting in a family of discrete rays per angle of incidence that defines a "refracted" scattering cone. The azimuth of rays were 0, 45, 90, 135, 180° relative to the orientation of the magnetic meridian (see Figure 34) with east or west azimuth providing identical loci for intersection between scattering cone and surface of the earth. While the magnetic field was used to define the scattering geometry, it was neglected in the computations for the rays. Rays were computed for all frequencies and azimuths cited earlier. Not all loci were plotted, however, in Figure 33. For certain combinations of frequency and azimuth, it was found that the scattering cones did not intersect the surface of the earth, for example, 24- and 30-MHz signals at azimuth 135°M . For the same frequencies arriving at an azimuth of 45°M , however, the signals are scattered to the ground south of Los Alamos.

For ionospheric conditions typical of autumn, local midnight, two intersections of the scatter cone including refraction are illustrated for 18 MHz and azimuths 90°M , 135°M . For the conditions chosen in Figure 33 it is seen that the locus of intersection for 18 MHz (135°M) differs significantly from that shown in Figure 35 for day versus night, 200 versus 250 km altitude, and assumed incident elevation angle $+5^{\circ}$ versus 0° . For local noon, autumn and a 200-km altitude at which signals at 12, 18, 24 and 30 MHz coming from an azimuth of 135°M are assumed to be incident on field-aligned irregularities. Figure 36

10. Miller, D.C., Gibbs, J. (1978) Ionospheric Modeling and Propagation Analysis, RADC-TR-78-163.

NOON
AUTUMN
200KM EL = 5°

P PLATTEVILLE, CO
A LOS ALAMOS, NM
B LOS BANOS, CA

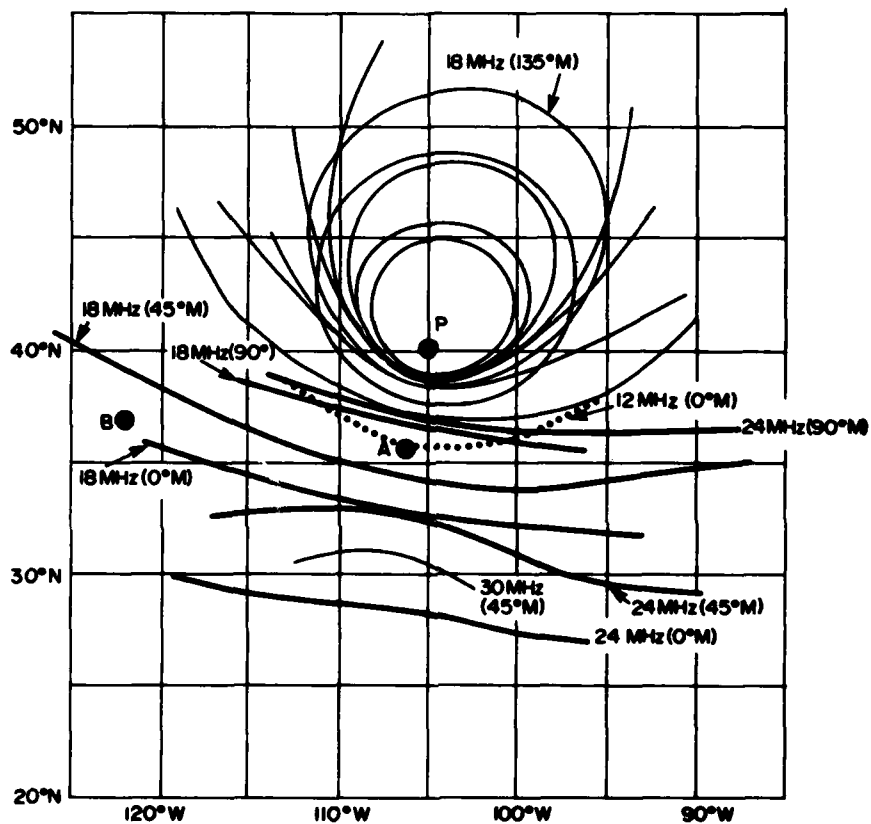


Figure 33. Loci of Scattering Cones, Including Refraction, Intersecting the Surface of the Earth. Scatter altitude: 200 km. Irregularities are field aligned, located above Platteville. Incident ray arrives at irregularity height with elevation angle of 5° from above the horizontal. Azimuth (AZ) of incidence is counted relative to magnetic meridian. This azimuth angle is zero if the ray arrives from the north in the plane of the magnetic meridian

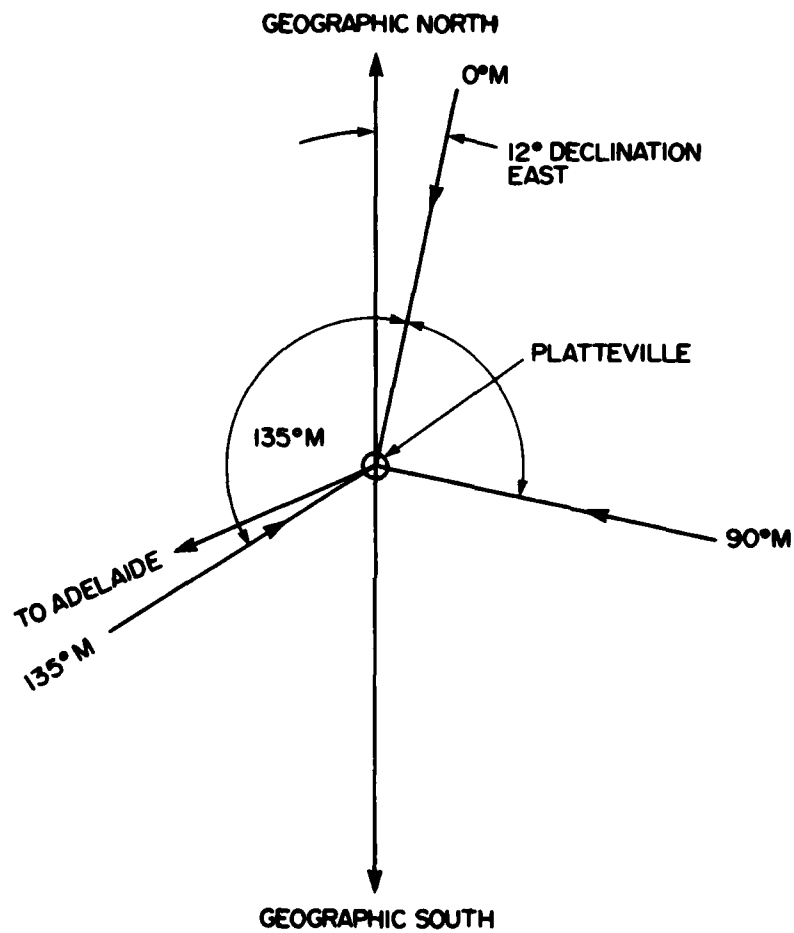


Figure 34. The Azimuthal Configuration Over Platteville, Colorado, Pertaining to the Scattering Loci, the Magnetic Meridian and the Direction Toward Adelaide, Australia

LOCAL MIDNIGHT (0700 U.T.)

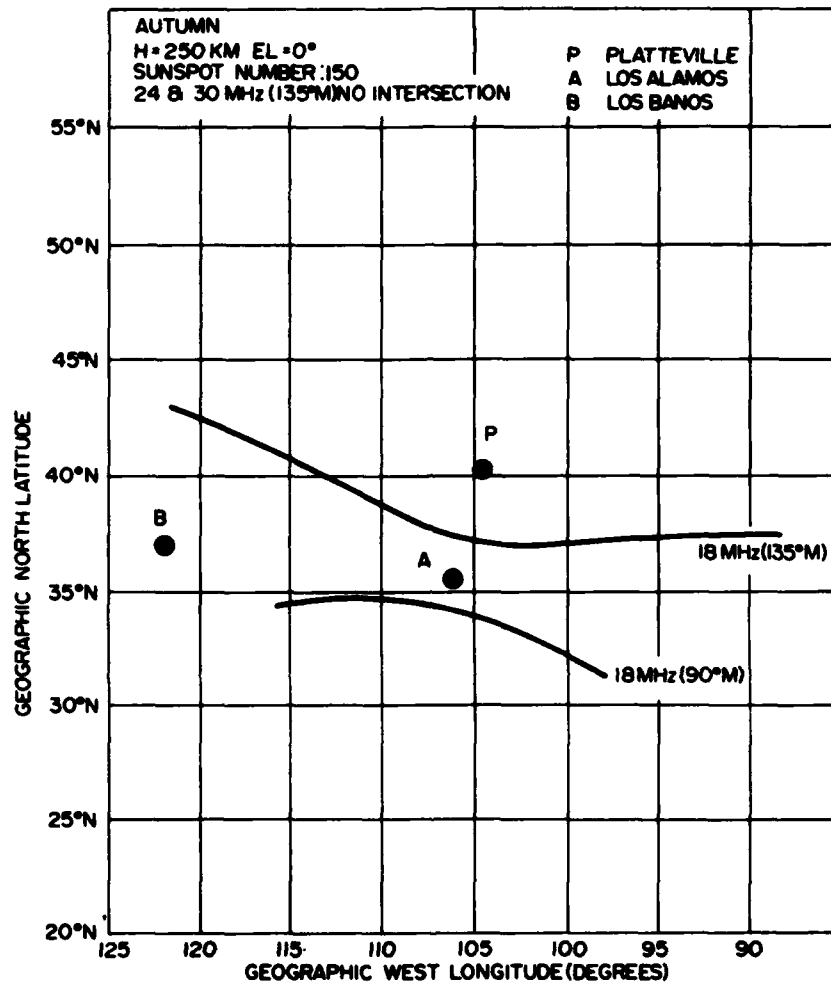


Figure 35. Loci of Scattering Cones with Refraction for $f = 18$ MHz and 2 Azimuths Illustrating the Location of the Loci North and South of Los Alamos

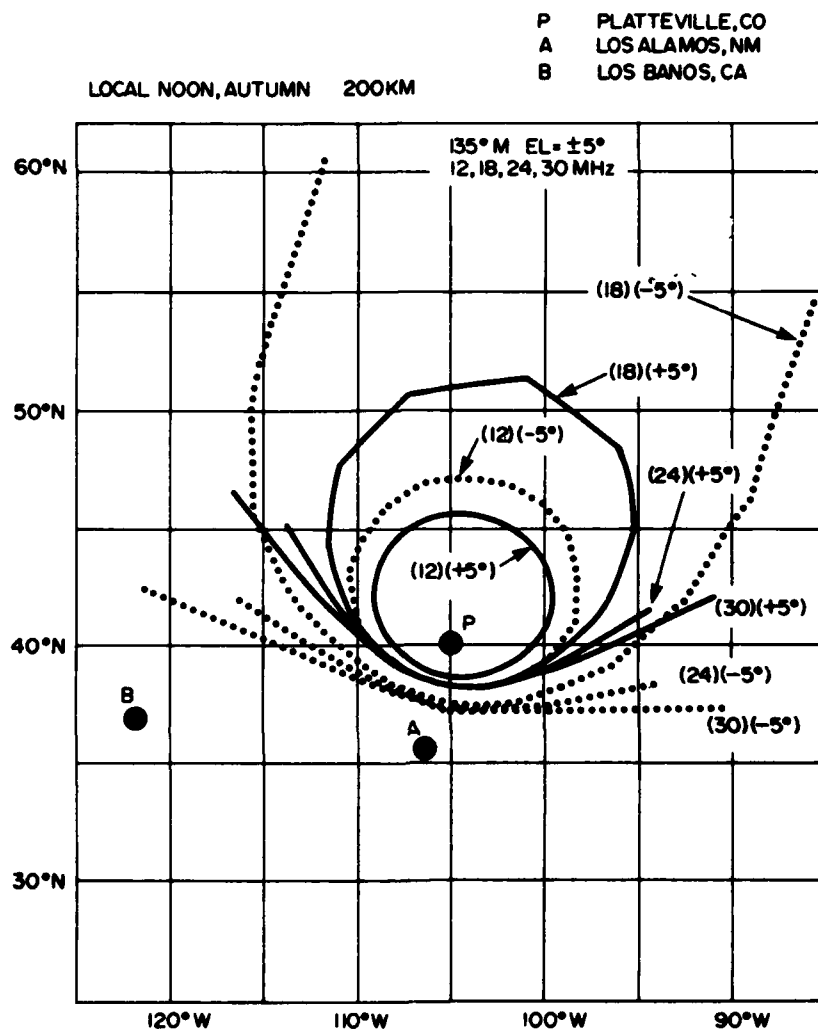


Figure 36. Effect of Elevation Angle of Ray Arriving at Irregularity Height with Elevation Angle of $+5^\circ$ (from above) and -5° (from below) With Respect to the Horizontal

illustrates the effect of elevation angle at the points of incidence above Platteville. The solid contours refer to arrival angle above the horizontal of $+5^\circ$, the dotted contours to -5° . For signals assumed to arrive from the south-west (135°M), a negative elevation angle of -5° displaces the intersection loci farther south from Platteville compared with a positive angle of $+5^\circ$. Higher frequencies tend to come farther south because they encounter reduced refraction.

Figures 33, 34 and 36 were based on simulation data derived from an ionospheric model¹⁰ that provided the geometry of the scattering contours. The results illustrate some characteristics of contours obtained by the choice of model ionospheres representing mean conditions. The choice of initial conditions for electromagnetic signals arriving at the field-aligned columns of the scattering volume resulted in an infinitesimal scattering cone that provided the initial conditions for computing the rays of which some reached the surface of the earth, while others did not.

The scattering geometry which is in principle characterized by the magnetic field of the earth is practically time invariant. In practice, ionospheric conditions will generally be different from the mean model used for computations. These changing conditions will influence the choice of heater frequency and thus the altitude at which field aligned irregularities are produced. Its consequence will be a set of different intersection loci originating now from a particular scattering cone located at some altitude with the landing of rays being subject to the prevailing refractive influences of the ionosphere.

3.2.1 MEASUREMENT CAMPAIGN OF 1978

During July and September 1978 measurements were made of the HF induced backscatter over Colorado¹¹ with an over-the-horizon radar at Lost Hills, and the Wide Aperture Research Facility (WARF) at Los Banos, both in California. The radar operated as a linear swept-frequency continuous wave (SFCW) backscatter sounder at frequencies from 6 to 30 MHz. The ionospheric modification was produced by the Platteville heater facility using 5 to 10 MHz as modifier frequencies. The most notable ionospheric effect of radio frequency heating is the creation of irregularities in the heater beam which are aligned in the direction of the earth's magnetic field. Narrow-band FM/CW transmissions (about 25-kHz bandwidth) were used to measure "cloud" echo strength resulting from the radar illumination of the irregularity volume and observe cloud cross-section changes caused by step-wise variations in the heater power levels. A difference in transmitted power of about 3.5 dB, resulting from cycling the RF heating power between 1.20 and 0.54 MW in 2 min intervals, resulted in a variation of echo power by about 2 dB

11. Showen, R.L., Zavoli, W.B. (1979) Platteville Heating Results: HF Radar Observations, SRI International, Tech. Report No. 43.

indicating a saturation with increasing HF power of the process causing the scatter.

At the WARF receiving site in Los Banos, the use of a hybrid spectrum analyzer provided real-time wide-sweep backscatter soundings to aid in optimizing the selection of transmissions and recording parameters. The receivers were operated with automatic gain control to accommodate the very large variation in received signal strength typical of wide-sweep soundings. To obtain azimuthal profiles of the "cloud's" cross section, three of the WARF's half-degree receive beams were repetitively stepped across a series of continuous bearings as the sounding frequency was varied. A WARF backscatter sounding ionogram showing "direct" scatter from the heated region is illustrated in Figure 37. Calibration markers were superimposed at intervals of 1 msec in time delay and 1 MHz in frequency corresponding to 10 seconds for the sweep rate of 100 kHz per second. Identifiable signatures in the sounding include the F-layer land-backscatter returns and direct echoes from the heated volume (cloud) over Platteville. The 2-MHz periodic structure seen in the "cloud" echo is the result of stepping the receive antenna beam in azimuth every 2.5 seconds corresponding to a 2-MHz interval. The echoes from the "cloud" seem to extend in frequency over the 16 to 30 MHz band. The mechanism of standard field-aligned scatter responsible for the cloud echoes led to absolute cross-section estimates of 10^8 square meters.¹¹ Although more information about the scattering cross-section is available, the cross-section estimates generally agree with earlier results.¹²

The computation of the apparent cross-section σ which includes an excess loss term that cannot be controlled or directly measured by the radar, was conveniently introduced. The equation for this quantity is

$$\hat{\sigma}_c = \frac{\sigma_c}{L} = S \frac{4\pi R^2}{P_t G_t} \cdot \frac{4\pi}{G\lambda^2} \cdot 4\pi R^2$$

where

σ_c = radar backscatter cross section of the "cloud"

L = excess loss

S = received signal strength

R = slant range

P_t = transmitted power

12. Fialer, P.A. (1974) Field-aligned scattering from a heated region of the ionosphere - Observations at HF and VHF, Radio Science 9(11):923-940.

G_t = receive antenna gain

λ = wavelength of sounding signal

$\hat{\sigma}_c$ = apparent cross-section $\left(\hat{\sigma}_c = \frac{\sigma_c}{L} \right)$

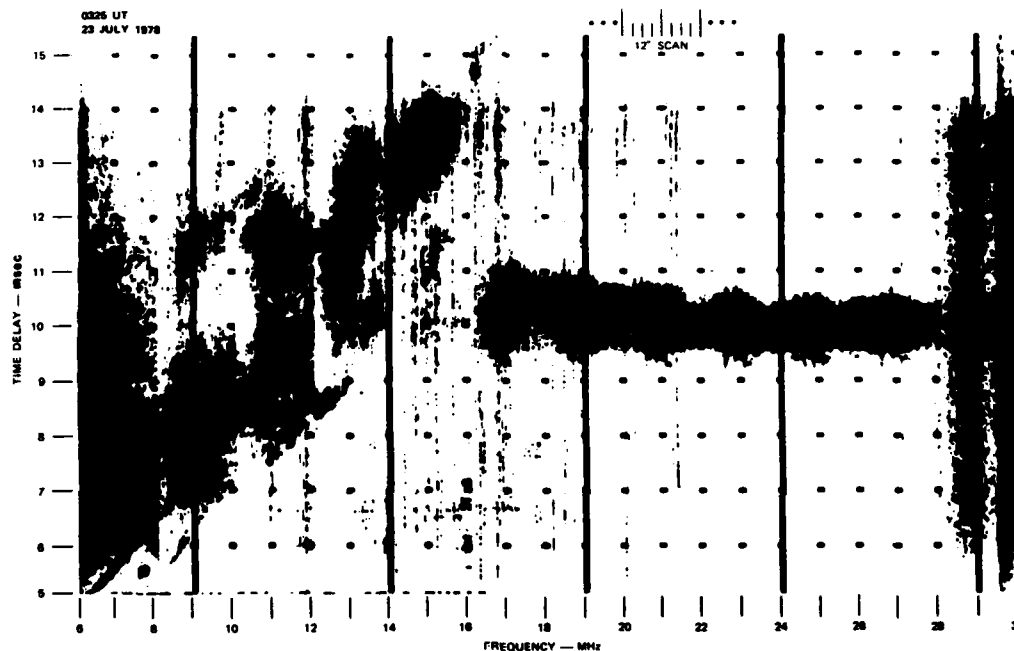


Figure 37. Wide Aperture Research Facility (WARF) Backscatter Sounding (Shows Direct Scatter From the Heated Volume Above Platteville and the Effects of Azimuthal Scanning on the Delay Spread)

3.2.2 MEASUREMENT CAMPAIGN OF 1979

3.2.2.1 Backscatter Ionograms

The second set of coordinated propagation experiments was conducted in April and June 1979 with RADC, Stanford Research Institute, International (SRI), Institute for Telecommunication Sciences (ITS) and the Australian transmitter taking part. Backscatter ionograms from the SRI transmitter at Lost Hills, its radiation scanning the heated volume over Platteville, were received/recorded at

Los Banos while the Platteville heater operated in an on-off power cycle.¹³ For frequencies ranging from 10 to 26 MHz, with transmission delays of about 10 msec corresponding to a range of 1500 km from WARF sites to Platteville, the echo from the heater induced irregularity volume (heater cloud) is readily apparent and quite strong. Figure 38 illustrates a nighttime ionogram that shows a heavy sloping band of signal returns from the ground after two reflections from the ionosphere representing ground backscatter, observable from about 6 to 17 MHz over a two-way transmission delay from about 5 to 20 msec. At a delay of 10 ± 0.8 msec the heater "cloud" is seen as a "direct" echo at a target range of 1500 km for frequencies from below 14 to above 21 MHz. For frequencies below 17 MHz the echo strength of the heater "cloud" may be partially suppressed due to capture of the receiver's automatic gain control by the relatively strong ground backscatter signal. In addition to the "direct" echo, the heater also produced a "cloud" echo at 13 msec delay time and at a frequency of 9 MHz which can barely be seen within the ground scatter. Based on earlier studies,¹⁴ this echo could be associated with a 1.5 hop propagation mode. Both echoes are composed of two returns each, analogous to the high- and low-angle rays of oblique propagation. Their relative strengths depend on the extent of defocussing encountered.

For comparison, no effect of the cloud is seen during the heater-off period at 0730 UT (Figure 38). The quasi-vertical-incidence traces on the lower left represent the ordinary-mode trace with a penetration frequency of about 6.7 MHz and the extra-ordinary mode trace of 7.3 MHz.

3.2.2.2 Australia to Platteville Transmissions (1979)

Frequency Modulation/Continuous Wave transmissions originating from Australia were received at Los Alamos while the Platteville heater operated in an on-off power cycle. It was anticipated that the successful reception of the Australian transmission at Los Alamos would make its presence over Platteville likely. There, and during the "heater-on" part of the cycle, electromagnetic energy would be scattered to the receiving system at Los Alamos, permitting deductions about the prevalent propagation mode.

Figure 39 illustrates the global layout of transmitting and receiving stations including a round-the-world great-circle path through Adelaide and Platteville. Portions of the path are marked in 2000-km increments. The path crosses the

13. Basler, Roy T., Showen, Robert L. (1979) Ducted Propagation in the Ionosphere for ICBM Surveillance Application, (U), SRI Int. Tech. Rep. 48, SRI Project, 4062; Contr. N000 14-75-C-0930. Funded by RADC/EEP through ONR NR086-876.
14. Bubenik, D.M. (1976) The Combined Effects of Refraction and Coherent Scattering by Columnar Ionization Density Irregularities in Ionospheric Radio Propagation, Stanford University, Stanford, California, Ph.D. dissertation.

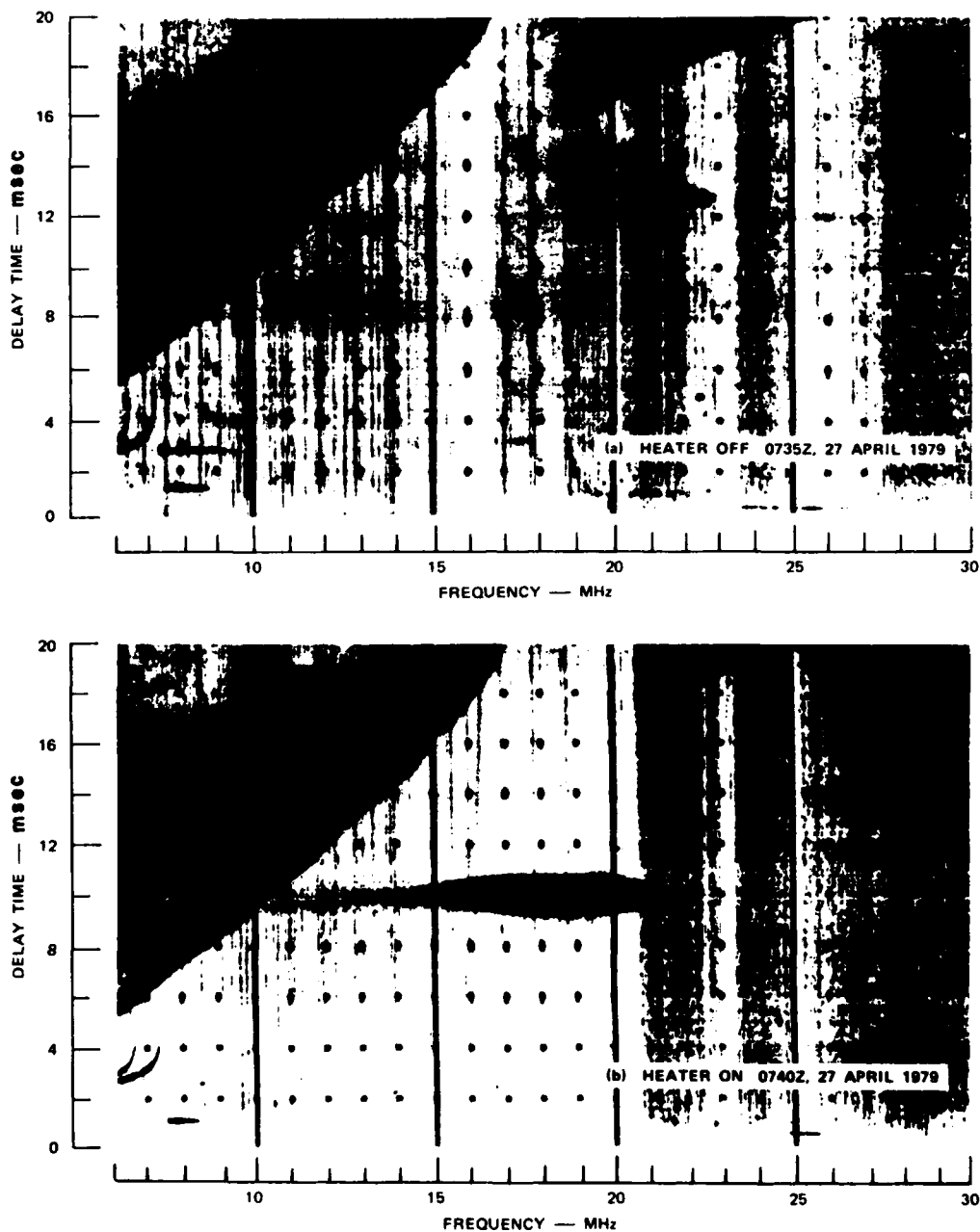


Figure 38. Nighttime Ionograms from SRI's Lost Hills Transmitter for 27 April 1979 (Shows Line-of-sight Echo from the Heated Volume above Platteville When the Heater is On (0740 UT) and Off (0735 UT))

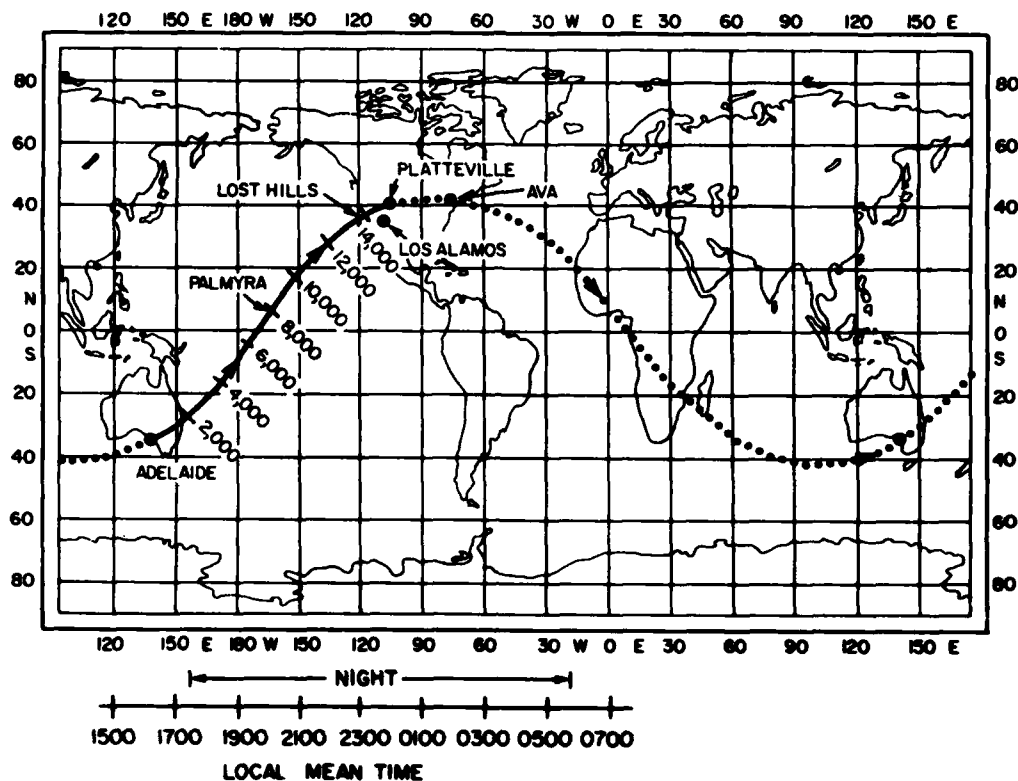


Figure 39. Map of the World Showing the Great-circle-path Defined by Adelaide and Platteville

equator at a distance of 6800 km from the location of the Australian transmitter. Conventional multi-hop-propagation between earth and ionosphere from Australia to Colorado is mostly over water. Near the equator, propagating signals are expected to encounter the equatorial anomaly. A particular local mean time is indicated on Figure 39 corresponding to 0700 UT. The day-night terminator is near the east coast of Australia. Most of the path to Platteville is in darkness.

The oblique ionogram in Figure 40 illustrates the hop conditions along the path from Australia to California, including the occurrence of propagation by way of reflection/scattering from the irregularity volume. About ten modes are shown for the time indicated, with a spread of about six milliseconds. When the heater is on, an additional propagation path comes into existence because of scattering off the "heater cloud." The arrival time of the scattered signal is delayed by 10 msec relative to the shortest "direct" path. The ionogram feature associated with the propagation from Australia to California, by way of the irregularity volume over Platteville, has a striking similarity to the corresponding feature of

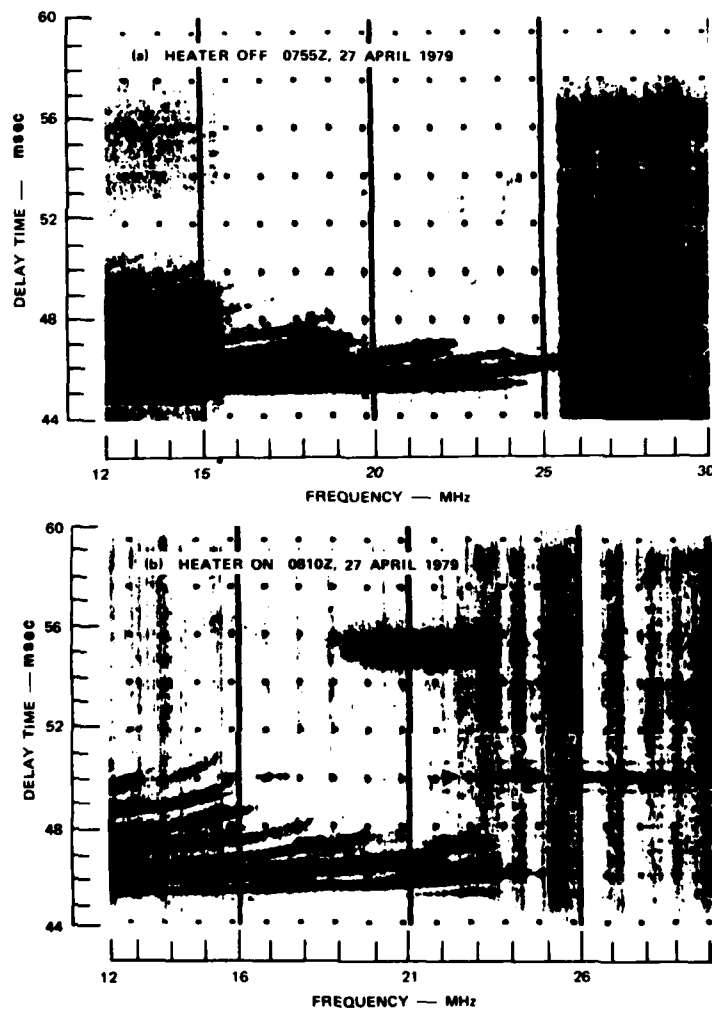


Figure 40. Oblique Ionograms for the Australia to Los Banos Propagation Path With Platteville Heater Off (top) and On (bottom)

the heater cloud with line-of-sight illumination observed from the WARF site (Figure 38). It was noted¹³ that the maximum frequency of the "cloud" echo was never seen above the maximum observed frequency for "direct" propagation at Los Banos. Moreover, the geometry is not favorable for signals coming from Australia and arriving horizontally (glancing incident) over Platteville, being scattered toward California. This fact, plus the observed limit in frequency of the echo from the heater cloud as seen at Los Banos, indicates that the Australian

signal, scattered from the irregularity volume over Platteville to Los Banos, did not propagate from Australia to Platteville in an elevated ducted mode, but rather in a conventional hop mode.¹³ From Figures 35 and 36 it may be surmised that Los Banos is indeed not likely to be found on loci of scattering cones of signals arriving over Platteville in elevated ducts.

The lower portion of Figure 41 displays an oblique ionogram for the transmission originating from Adelaide, Australia as received at Los Alamos over a surface distance of about 14,255 km. This ionogram was obtained on 27 April 1979 during the time interval 0800 to 0802 UT corresponding to 0100 to 0102 LT at Los Alamos and 1700 to 1702 LT at Adelaide. The propagation path is essentially in darkness and the "terminator" is near and east of the transmitter. Signals originating from Adelaide and propagating northeast into nighttime ionosphere toward Los Alamos and Platteville, encounter negative horizontal ionization gradients (Figure 42). In terms of ray refraction, such gradients are favorable for injection of a family of rays into existing elevated ducts in which signals propagate over large distances for as long as the duct is effectively maintained in range, and with attenuation far below that expected for multi-hop propagation between earth and ionosphere involving multiple traverses of the absorbing D region.

At least 11 multi-hop modes are shown on the lower left of Figure 41 spread over a 5 msec delay. Relative delay is read along the ordinate from about 48 to 55 msec. The time delay between Salisbury and Los Alamos, resulting from pulse signal propagating along the surface of the earth over a great circle path with the velocity of light, c , in free space is obtained dividing the great-circle distance by c . The shorter great-circle distance between Adelaide and Los Alamos was estimated to be 14,255 km corresponding to a time delay of 47.51 msec. With perfect time synchronization between the standard clocks at the Adelaide transmitter and Los Alamos receiver, one would be able to place correctly absolute-delay time markers along the ordinate. This would allow one to determine the delay in the arrival of the earliest earth-ionosphere hop mode. For relatively uniform and undisturbed ionospheric conditions the knowledge of absolute time could facilitate mode identification.

The echo trace extending in frequency from about 18 to 28 MHz and centered on a relative delay of about 52 msec throughout this frequency range with delay spread of one msec, is the result of scattering to Los Alamos of the "Adelaide" signal from the ionospheric irregularity volume over Platteville. This echo trace represents a feature of those oblique ionograms that were recorded while the Platteville heater was on. In contrast, the upper portion of Figure 41 illustrates an ionogram taken 5 min earlier when the Platteville heater was off. Unrelated to the heating process, a change in the hop-mode structure with respect

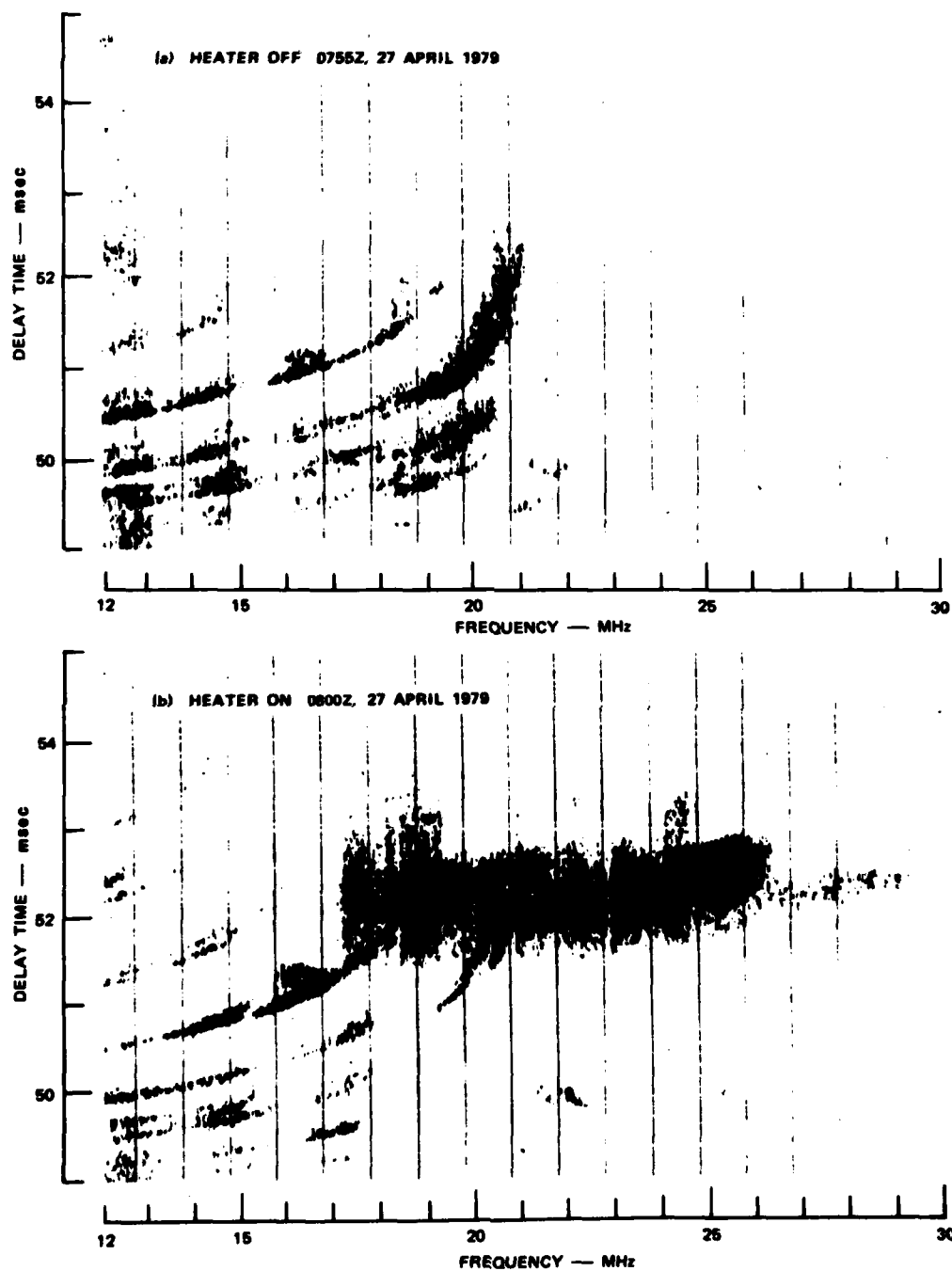


Figure 41. Oblique Ionograms for the Australia to Los Alamos Propagation Path with Platteville Heater Off (top) and On (bottom)

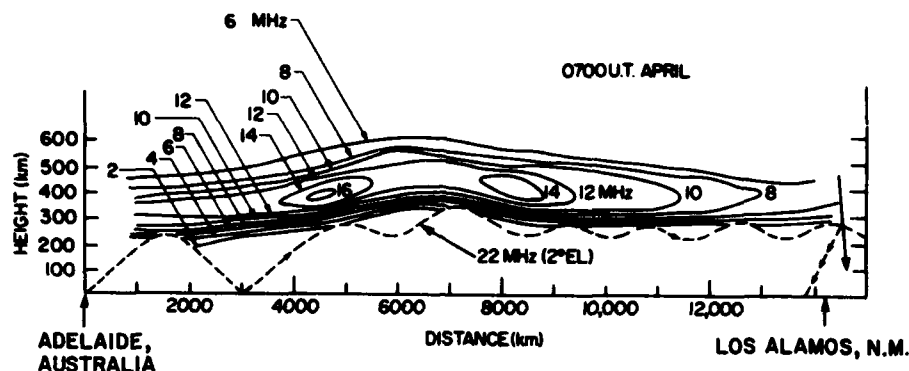


Figure 42. Ionospheric Contours Characterized by Plasma Frequency in Megahertz, Derived From Ionospheric Model IONCAP for April, 0700 UT for the Path from Adelaide, Australia to Los Alamos, New Mexico. A ray launched with 2° elevation angle at a frequency of 22 MHz is ducted after one hop from the transmitter

to that shown the lower portion of Figure 41 is the result of naturally occurring ionospheric changes over this super-long propagation path. The echo trace previously identified and caused by heating of the ionosphere over Platteville is now absent.

4. ANALYSIS AND INTERPRETATION

Several propagation measurement campaigns have been conducted in conjunction with the use of the Platteville heater for modifying the ionosphere, in order to verify the scattering geometry, determine scattering cross section and attempt to extract ducted modes having propagated over great distances. These campaigns provided a basis for inferring that ducted modes, scattered by the irregularity volume, have been detected on the ground. It was pointed out¹³ that a mode scattered from the irregularity volume over Platteville to a receiver (at Los Alamos), where also regular (direct) multi-hop earth-ionosphere modes are recovered, is likely to have been ducted if its trace on the oblique ionogram extends beyond the maximum observable frequency of the multi-hop mode of the lowest order (Figure 41). If the maximum observable frequency of the lowest-order hop mode is not exceeded by the signal scattered from the heated volume, it can be assumed that the scattered signal (Figure 40) had arrived at the heated volume by regular hop modes.

Raytracing computations corresponding to the Australia-Platteville/Los Alamos path were made at the Institute for Telecommunications Sciences. Figure 42 represents ionospheric contours for April, 0700 UT, characterized by plasma frequency in megahertz. These contours were provided by the ITS program IONCAP.¹⁵ The Australian transmitter is located at the origin ($D = 0$). Rays are launched at an azimuth of 65° East of North along a great-circle path toward Platteville. Transmission from Adelaide toward the East at 0700 UT encounters a nighttime ionosphere with gradients favorable for the injection of rays into the existing ducts. The F-region anomaly is seen having plasma frequencies of 16 MHz at $D = 4500$ km and 14 MHz at $D = 8400$ km. A trapped ray of $f = 22$ MHz and launch elevation angle of 2° is illustrated. Other rays were computed for 26 MHz with 14° and 16° elevation angles at launch. Ducted modes were obtained in all three cases. Rays arriving over Platteville encounter heater-induced field-aligned irregularities, that scatter radio energy to the ground. A comparison of the experimental results of Figure 41 and the ray computations of Figure 42 provides reasonable certainty that a ducted propagation mode was scattered toward the receiving site at Los Alamos.

5. CONCLUSION

In this report theoretical considerations were presented and illustrated to describe expected characteristics of trapped modes in the ionosphere. Computational raytracing through realistic ionosphere models confirmed that under favorable gradient conditions and for certain frequencies and launch angles, rays can enter elevated ionospheric ducts and remain trapped over large distances. Experimental evidence of scattering from artificially created ionospheric irregularities showed that modes trapped in such elevated ionospheric channels can be detected on the ground at locations that generally satisfy the geometry for scattering from field-aligned irregularities.

While these ground-based measurements have provided new understanding and evidence for ionospheric ducting, the experimental configuration was fixed and thus limited. A new approach is presently envisioned and plans have been implemented to conduct a ducting experiment using a ground-based transmitter

15. Lloyd, John L., Haydon, George W., Lucas, Donald L., Teters, Larry R. Estimating the Performance of Telecommunication Systems Using the Ionospheric Transmission Channel, Vol. 1, Techniques for Analyzing Ionospheric Effects Upon HF Systems (to be published by NTIA/ITS).

with the receiver, mounted on a space vehicle, orbiting at altitudes of the ducting channel. It will then be possible, for the first time, to measure in situ the extent of ducting in ionospheric channels, and the properties of ionospherically ducted modes.

References

1. Tushentsova, I.A., Fishchuk, D.I., Tzedilina, Ye. Ye. (1975) Investigation of the global properties of ionospheric wave ducts, 2, Geomagn. Aeron. 15(1):62-66.
2. Toman, K., Miller, D.C. (1977) Computational study of long-range high-frequency ionospheric ducting, Radio Science 12(3):467-476.
3. Gurevich, A.V., Tzedilina, Ye. Ye. (1976) Trapping of radiation in the ionospheric duct during scattering on artificial inhomogeneities, Geomagn. Aeron. 15(6):713-715.
4. Gurevich, A.V. (1971) Effect of nonlinearity on the generation of circum-terrestrial signals, Geomagn. Aeron. 11(6):810-817.
5. Vever, A.S., Danilova, T.P., Shlionsky, A.G. (1978) Possibility of the trapping of radio waves, scattered by meteor trails, by ionospheric ducts, Geomagn. Aeron. 18(3):306-308.
6. Erukhimov, L.M., Matyugin, S.N., Uryadov, V.P. (1975) Radio wave propagation in ionospheric wave channels, Radiophysics & Quantum Electronics 18(9):958-963.
7. Rush, C.M., Elkins, T.J. (1975) An assessment of the magnitude of the F-region absorption on HF radio waves using realistic electron density and collision frequency models, ITU Telecommunication Journal, Geneva.
8. Toman, K. (1979) High-frequency ionospheric ducting - A review, Radio Science 14(3):447-453.
9. Golyan, S.F. (1975) Optimal conditions for extra-long-range short-wave propagation, Radiophysics & Quantum Electronics 18(9):1014-1022
10. Miller, D.C., Gibbs, J. (1978) Ionospheric Modeling and Propagation Analysis, RADC-TR-78-163.
11. Showen, R.L., Zavoli, W.B. (1979) Platteville Heating Results: HF Radar Observations, SRI International, Tech. Report No. 43.

12. Fialer, P.A. (1974) Field-aligned scattering from a heated region of the ionosphere - Observations at HF and VHF, Radio Science 9(11):923-940.
13. Basler, Roy T., Showen, Robert L. (1979) Ducted Propagation in the Ionosphere for ICBM Surveillance Application, (U), SRI Int. Tech. Rep. 48, SRI Project, 4062; Contr. N000 14-75-C-0930. Funded by RADC/EEP through ONR NR086-876.
14. Bubenik, D.M. (1976) The Combined Effects of Refraction and Coherent Scattering by Columnar Ionization Density Irregularities in Ionospheric Radio Propagation, Stanford University, Stanford, California, Ph.D. dissertation.
15. Lloyd, John L., Haydon, George W., Lucas, Donal L., Teters, Larry R. Estimating the Performance of Telecommunication Systems Using the Ionospheric Transmission Channel, Vol. 1, Techniques for Analyzing Ionospheric Effects Upon HF Systems (to be published by NTIA/ITS).



MISSION of Rome Air Development Center

RADC plans and executes research, development, test and selected acquisition programs in support of Command, Control Communications and Intelligence (C³I) activities. Technical and engineering support within areas of technical competence is provided to ESD Program Offices (POs) and other ESD elements. The principal technical mission areas are communications, electromagnetic guidance and control, surveillance of ground and aerospace objects, intelligence data collection and handling, information system technology, ionospheric propagation, solid state sciences, microwave physics and electronic reliability, maintainability and compatibility.